Sub-picosecond C=C bond photo-isomerization: Evidence for the role of excited state mixing

Damianos Agathangelou, Partha Pratim, María del Carmen Marín, Nicolas Ferré, Massimo Olivucci, Tiago Buckup, Jérémie Léonard, Stefan Haacke

Sub-picosecond C=C bond photo-isomerization: Evidence for the role of excited state mixing

Photo-isomérisation sub-picoseconde de liaisons C=C: L'importance du mélange des états excités

Damianos Agathangelou[1,*], Partha Pratim Roy[2,†], María del Carmen Marín[3], Nicolas Ferré[4], Massimo Olivucci[3,5], Tiago Buckup[2], Jérémie Léonard[1], Stefan Haacke[1]

[1] Université de Strasbourg – CNRS, Institut de Physique et Chimie des Matériaux de Strasbourg, 67034 Strasbourg, France

[2] Physikalisch-Chemisches Institut, Ruprecht-Karls Universität Heidelberg, 69120 Heidelberg, Germany

[3] Biotechnology, Pharmacy and Chemistry Department, University of Siena, Siena 53100, Italy

[4] Aix-Marseille Univ. - CNRS, ICR, 13397 Marseille, France

[5] Chemistry Department, Bowling Green State University, Bowling Green, Ohio 43403, United States

Abstract

Sub-picosecond photo-isomerization is the major primary process of energy conversion in retinal proteins and has as such been in the focus of extensive theoretical and experimental work over the past decades. In this review article, we revisit the long-standing question as to how the protein tunes the isomerization speed and quantum yield. We focus on our recent contributions to this field, which underscore the concept of a delicate mixing of reactive and non-reactive excited states, as a result of steric properties and electrostatic interactions with the protein environment. Further avenues and new approaches are outlined which hold promise for advancing our understanding of these intimately coupled chromophore-protein systems.

Résumé

La photo-isomérisation sub-picoseconde est la principale réaction initiant la conversion d'énergie dans les protéines de rétinal, si bien qu'elle fait l'objet de travaux théoriques et expérimentaux approfondis depuis plus de trente ans. Dans cet article de revue, nous revisitons la question toujours ouverte de savoir comment la protéine détermine la vitesse d'isomérisation et son rendement quantique. A la lumière de nos contributions récentes en ce domaine, nous décrivons le concept d'un mélange d'états excités réactifs et non-réactifs, délicatement ajusté par les interactions stériques et électrostatiques avec l'environnement

[*] Now at : LUMOS lab, University of Michigan, Department of Physics, USA

[†] Now at : University of Berkeley, Department of Chemistry, USA

protéique. De nouvelles perspectives et approches prometteuses sont décrites qui pourront faire progresser la compréhension de ces systèmes chromophore-protéine intimement couplés.

Keywords: Photo-isomerisation, retinal proteins, chromophore-protein coupling, non-adiabatic dynamics, photo-sensory proteins, charge transfer state

Many organisms, from microbacteria to vertebrates, use photosensitive retinal proteins for photo-chemical energy conversion or photo-sensory functions [1–3]. Visible light-absorbing retinal proteins rely on the protonated Schiff base of retinal (rPSB) as chromophore, covalently bound to the interior of a barrel-like "opsin" protein. Their biological activity is triggered by a regioselective and stereoselective C=C double bond photoisomerization of rPSB, e.g. 11-*cis* to all-*trans* for the visual pigment rhodopsin (Rho), all-*trans* to 13-*cis* for the proton pump bacteriorhodopsin (bR), or both 13-*cis* to all-*trans* and all-trans to 13-*cis* for the bistable, photochromic Anabaena Sensory Rhodopsin (ASR). In all cases, the protein scaffold exerts electrostatic and steric interactions on the chromophore [4–7], which tune the rPSB photoreaction dynamics, e.g. the excited state lifetime (ESL) and its photoisomerization quantum yield (IQY), ultimately determined by the branching ratio between reactive and non-reactive channels. The pronounced influence of the protein interaction on rPSB photo-reactivity is evidenced by comparing with the photoreaction dynamics and IQY of rPSB in other environments, e.g. in solution [8–14] or in vacuum [15].

The photoisomerization of rPSB occurs through a conical intersection (CInt), [16,17] which is an intersection seam between the excited (S_1) and ground (S_0) state potential energy surfaces (PES), where the molecule transiently adopts a configuration with a nearly 90° twisted reacting double bond. While it has been shown that there is no correlation between ESL and IQY [18–21], many theoretical predictions agree, that the PESs topography and the nuclear motions at the CInt decide on the branching between reactive and non-reactive pathways, hence on the overall IQY [17,22,23]. There is large scientific interest at investigating the photoreactions of retinal proteins in order to decipher the intra- and inter- molecular parameters which tune the photoreactivity of rPSB, as a model system for non-adiabatic dynamics through a CInt. In addition, such a fundamental understanding would be the key to define chemical design strategies to control the photoreactivity of C=C double bond isomerization in retinal chromophores or similar compounds. In particular, there is broad interest in producing rhodopsin mutants with an enhanced ESL and, as a consequence, fluorescence quantum yield (FQY) for applications in optogenetics [24,25]. Moreover, understanding the dynamic structure-property relationships will most likely indicate new avenues for tailoring molecular devices based on ultrafast C=C double isomerization to perform photoswitching or rotary motion, at the molecular scale, with optimum efficiency [26].

Chapter I gives a brief and necessarily incomplete account of recent experimental studies on the effect of the environment of the photophysics of rPSB's, with an emphasis on the electrostatic properties, in particular the presence or protonation state of counter ions.
Chapters II to IV concentrate on both electrostatic and steric effects on the ESL and FQY of rPSB in different retinal proteins and rhodopsin-mimicking photo-switches in solution. Steric effects, in particular the distortion of the rPSB in the ground state of 11C in Rho as opposed to the more planar AT in bR is held responsible for the faster photo-isomerization reaction in Rho [27–32], as will be corroborated in these chapters. In chapter II, we review the concept of $^1B_u/^2A_g$ mixing between the first two excited states (**Error! Reference source not found.**), and how it translates both steric and electrostatic properties comprehensively. Chapter III then treats the experimental manifestation and quantitative explanation of these effects for *Anabaena Sensory Rhodopsin* and some selected mutants. Chapter IV extends this combined treatment to rhodopsin-mimicking photo-switches, before chapter V summarises the main concepts and outlines future avenues.

I. An open question studied on different systems

The protonation of the retinal Schiff base in VIS-absorbing retinal proteins makes these systems distinctively different from their UV-absorbing sisters, which function with a deprotonated chromophore [33]. The charge-transfer character of the lowest excited state [34,35], S_1, is at the heart of the high sensitivity to the presence of counter ions and dynamic

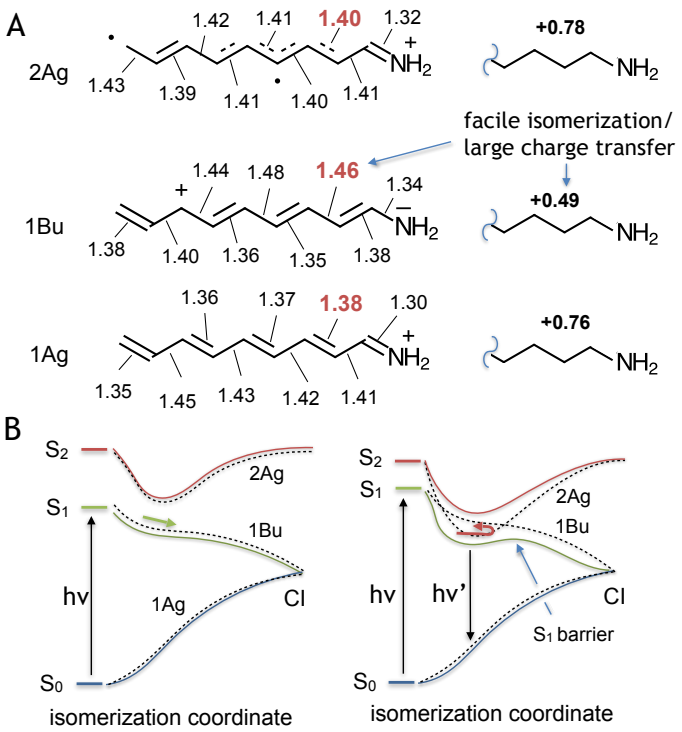

Figure 1: Schematic representation of A: the charge transfer character and bond length alternation (BLA) of the most relevant electronic states S_0, S_1 and S_2 of rPSB in Franck-Condon geometry, and B : Two extreme cases of weak and strong mixing of the ^1B_u and ^2A_g character of the first two excited states, presented together with S_0 as a function of an effective isomerization coordinate, limited to the first 90° rotation of the reactive double bond (see also fig. 11). Note the conical intersection (CI) between S_1 and S_0. Refer to chapter II for a more detailed discussion.

electrostatic interactions, thereby controlling the excited state dynamics. This will be highlighted in the following paragraphs.

a. Isolated rPSB's in solution and gas phase

Since 11-*cis* (11C) and all-trans (AT) isomers are the ground state conformations of the visual photo-receptor and of the large majority of microbial retinal proteins, respectively, these were studied quite extensively as isolated molecules in solution and to a lesser extent in the gas phase. It was first noticed that the absorption spectra in solution are significantly blue-shifted with respect to the situation in protein cavities (referred to as the "opsin shift"). It can be quantitatively explained by a stronger polarizability of the protein environment and interaction of the rPSB with its counter ion in solution, reduced though for polar solvents, and, for AT rPSB, by an enhanced ring/chain co-planarization in proteins [36–39]. In solution, the 11-*cis* isomer photo-isomerization produces specifically the AT isomer, like in proteins. The IQY is however only about 25% in various solvents versus 67% in Rhodopsin. Conversely, the photo-isomerization of AT in solution produces a variety of product isomers, unlike in proteins where it is 100% bond-selective, and occurs with a total IQY in the range of 15% [40–42].
Femtosecond transient absorption and fluorescence spectroscopy consistently showed that the excited state lifetimes and thus the isomerization times are significantly longer than in proteins, with a dominant decay component in the 3-4 ps range, for both the 11C and AT rPSB's [8,10,12,43–45]. For AT, sub-picosecond fluorescence decay components were attributed to internal conversion and the dominant non-reactive back reaction [10,21]. The ESL increase at lower temperatures points to the existence of a small excited state barrier [12]. Conversely, in the case of 11C in solution, the sub-ps component was attributed to the minority, barrier-less reactive channel while the 4-ps component would characterize the dominant non-reactive channel [45].

In the absence of a counter ion or any polarisable environment, i.e. for rPSB's in gas phase, the absorption spectra of AT and 11C rPSB's are red-shifted with respect to the protein spectra, due to a relative destabilisation of S_0 [46,47]. The energies of the UV/VIS electronic transitions are obtained by recording the photo-fragmentation action spectra of the cationic chromophores held in an ion storage ring. Recently, this approach was extended to two-pulse experiments, which allowed to record the excited states lifetimes *in vacuo* [15]. A first pump pulse resonantly tuned onto the S_0-S_1 transition excites the molecules, and, after a delay time τ, a second pump pulse at 800 nm promotes the molecules further to S_3. This additional excess energy stored in the molecule leads to enhanced photo-fragmentation, as compared to the pump pulse-only case. Due to the limited ESL, the fragmentation enhancement is dependent on τ, and the delay-dependent signal measures the time-dependent fraction of excited molecules. A series of comparative experiments, including the effect of temperature concluded that, *in vacuo*, 11C rPSB has an almost barrierless fast decay (≈ 0.4 ps at room temperature), while AT shows a barrier-controlled > 3 ps decay.

Hence, both solution and gas phase experiments suggest, that in visual rhodopsin the ESL is inherited from the "intrinsic" properties of the 11C chromophore [15,45], whereas in bacterial rhodopsins, the protein tunes the excited state potential energy surfaces (PES) of AT in terms of barrier height and bond selectivity [15,44]. The origin of these environment-induced modifications of the PES will be discussed in detail in chapter II, on the basis of computational results involving mixing of the first two excited states. While such modelling allows rationalizing the effect of the protein environment on the ESL, the question about how the

proteins tune the IQY of 11C and AT chromophores remains largely open. So far, only in the unique case of rhodopsin – showing the fastest photoisomerization reaction - a direct connection was established between the specific vibrational motions driven by the PES topography and the IQY, pointing to the central role of the relative phase between a few essential vibrational modes at the moment of decay at the CInt [23].

b. *Effects of mutations and pH on excited state dynamics of retinal proteins – a selection*

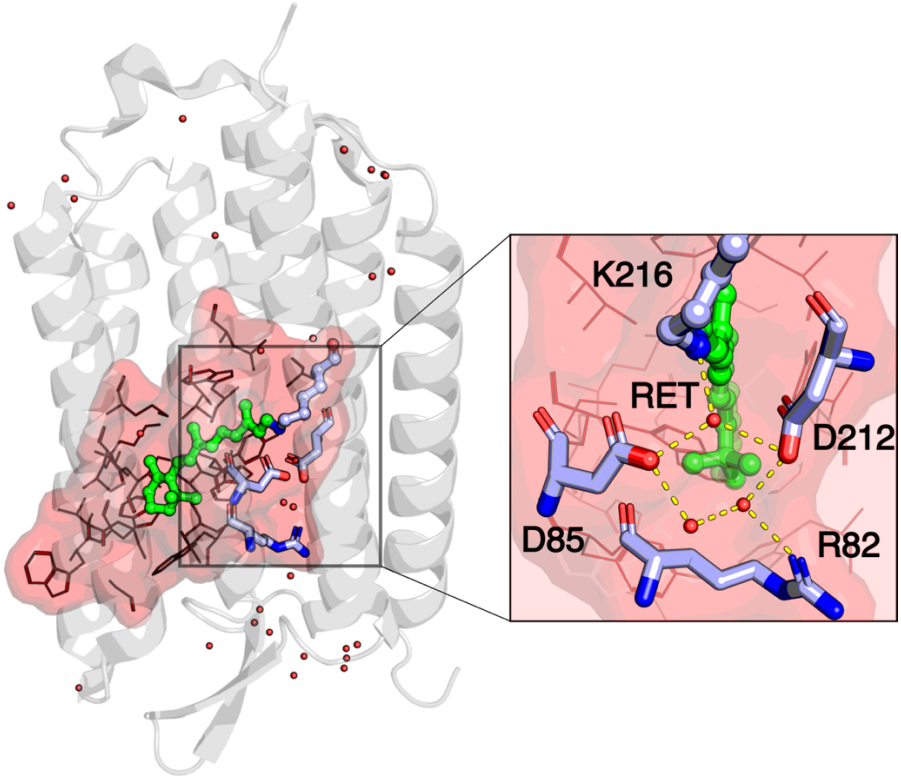

Figure 1: Crystallographic structure of bR (pdb entry 5ZIL), at pH=7, highlighting the retinal chromophore RET (green), covalently bound to Lys216 (blue). The protonated Schiff base linking Lys216 and RET, is connected to the counter ion, the deprotonated aspartic acid D85, via a water molecule. Right : The zoom shows the H-bonding network involving three waters and key residues. Their effects on bR's ESL and IQY was studied by femtosecond spectroscopy (see text).

The most studied microbial rhodopsin is bR, a light-activated proton pump, found in *Halobacterium salinarum* [48]. In its light-adapted form, it binds the rPSB primarily in the AT form. In wild-type bR, AT→ 13C photo-isomerization occurs within ≈0.5 ps [49–52], and with a quantum yield of ≈65% [53–55]. As shown in Figure 1, the crystallographic structure, at pH=7, identifies the deprotonated aspartic acid D85 as the main counter ion of the rPSB connected via a H-bond network with D212 and R82 via three water molecules [28]. First experimental work by El-Sayed and Lanyi [56,57] reported that the replacement of charged residues in the mutants D85N, D212N and R82Q by neutral ones increases the excited state lifetime and thus isomerization time by a factor of 5 to 20. Replacements of uncharged residues in mutants D115N or Y185F did not change the lifetimes significantly. The exact analysis was complicated by the fact that mutations, much like acidification [58], induce a mixture of AT and 13C isomers in the ground state. The observations were explained by a valence bond resonance model describing the excited state as a linear combination of wavefunctions, the electronic densities of which have the positive charge translocated from the Schiff base to different C atoms with odd numbers along the polyene chain. This provokes for every ground state double bond a

reactive single bond character in the excited state, but depending on the fraction of local positive charge. Due to the nearby negatively charged D85 and D212, the positive charge is stabilised best on C13 in the excited state of wild-type bR, providing an intuitive explanation of the bond selectivity of the AT→ 13C isomerization process. The excited state single bond character of C13=C14 allows then for a barrierless and therefore ultrafast isomerization. These effects are absent when D85 and D212 are replaced by neutral residues or if they are protonated (neutral) as in R82Q at pH=4 [56]. The results for D85N were later confirmed and complemented by femtosecond photon echo spectroscopy, which provided evidence for a large sub-100fs dielectric relaxation of the protein environment [59].

Another more recent example for large effects on ESL and IQY related to the chromophore environment, was recently reported for KR2, from *Krokinobacter eikastus*. In 2013, it was discovered as the first light-activated Na^+ pump [60]. Its crystallographic structure was resolved [61,62], highlighting particular motifs responsible for Na^+ binding at the protein periphery, and most importantly a transient Na+ binding site, in the vicinity of the rPSB, made up of D116, N112 and D251, and, with respect to bR, a modified H-bonding network. Comparing the crystal structures at neutral and acidic pH allowed to identify the flipping of the retinal counterion, the aspartic acid D116, as a key element for Na^+ pumping. At neutral pH, D116 is H-bonded with retinal's Schiff base (rotamer 1), but during the M intermediate of KR2's photocycle, protonation of D116 via the Schiff base (SB) occurs. This would lead to its re-orientation (rotamer 2) and disruption of the otherwise strong H-bonding network, thus enabling Na^+ translocation [61]. The overall structural changes associated with Na^+ pumping were very recently analyzed by time-resolved serial X-ray crystallography and QM/MM simulations, covering the pico- to milli-second time scales [63]. However, the changes in the SB-D116 distance were observed to be much smaller than expected, and no clear evidence for the existence of two rotameric states was found in the photocycle at pH=8.0.

Regarding ultrafast events, Hontani et al. reported a spectroscopic investigation of the full photo-cycle, and in particular the primary AT→ 13C isomerization to occur in KR2 within ≈ 200 fs, at pH=8.0 [64]. This is significantly faster than for other microbial rhodopsins bearing AT rPSB in the ground state and was attributed to steric effects, i.e. distorsion of the AT isomer [65]. Tahara et al. investigated the effect of pH on the primary photo-reaction by femtosecond transient absorption spectroscopy (TAS) [66], with the main objective of obtaining new insights into minority excited state species with > 3 ps lifetimes observed at pH=8.0 [65]. Protonation of D116 occurs for pH< 7, and leads to a significant red-shift of the absorption spectrum [60], due to destabilization of the protonated SB ground state (S_0). KR2 at pH<7 and the D116N mutant show several ps excited state decay components, in addition to the 0.18 ps ESL, whose amplitudes increase for lower pH values. The opposite is observed for pH >7. A good correlation with the pH-dependent IQY showed that only the 0.18 ps decay channel is productive in terms of isomerization. A more detailed analysis of the data suggests that, rather than the protonation state of D116N, the key parameter favoring the fast and efficient excited state pathway is the orientation of that residue and its fraction of population able to form H-bonds with retinal's Schiff base [66]. While a similar co-existence of multiple excited state decay components was previously attributed to reactive and non-reactive excited state pathways [21,44,56,67,68], this study points to the central role of structural inhomogeneities in the ground state, modulated by the protonation of D116N. Similar conclusions were recently drawn by the same authors for the photo-isomerization reactivity in proteorhodopsin [69]. In conclusion, KR2 appears to be a particular retinal protein, affording a flexible and thus disordered Schiff base environment, required for the binding of Na^+, but at the cost of a

relatively low isomerization IQY. Nevertheless, intensive research is under way to use KR2 as a platform for genetic modifications in view of applications in optogenetics [3,24,70,71].
Last but not least, it is worth noting that the protein environment should not be considered as a rigid grid of point charges. In addition to ultrafast nuclear motion of the surrounding residues and their related charges [72,73], several experiments performed on bR point to a dynamic electronic response, upon excitation of rPSB, in particular for the polarisable nearby Trp residues, such as Trp86 [74–76]. From a computational point of view, these effects would require a quantum mechanical treatment of the large "rPSB/polarizable residue" system [73] and are out of the scope of the present review.

II. Theoretical framework: Potential energy surfaces and CInt

Since the rPSB is a special case of a linear polyene chain, the role of possible interactions of the first and second excited states (S_1 and S_2) has been frequently evoked and examined in the past [5,77–82]. Adopting the symmetry nomenclature of polyenes, the electronic ground state is referred to ^1Ag, and the first excited states to ^1B_u and ^2A_g symmetry (cf. **Error! Reference source not found.**), even though the chromophore is asymmetric due to the positive charge on the Schiff base end. Hence, at the FC point (i.e., at the S_0 equilibrium structure), S_0 has ^1A_g covalent character with alternating single/double bond lengths, and a positive charge located on the $C=NH_2$ framework end. With respect to the ground state, the ^1B_u state can be described by a bonding π to an anti-bonding $\pi*$ electronic transition, delocalized all over the retinal backbone. Such a modification triggers a substantial structural change, characterized by single and double bond inversion (cf. **Error! Reference source not found.**), hence the bond length alternation (BLA, defined as the average single bond length - average double bond length) changes sign. Negative BLA is necessary for the isomerization to occur, i.e. ^1B_u is the reactive configuration. In addition, the state has a pronounced charge-transfer (CT) character, which implies that the positive charge on the $C=NH_2$ framework end is reduced and translocated to the polyene backbone. By contrast, the S_2 PES has ^2A_g diradical (DIR) character with a strongly reduced BLA. Compared to ^1B_u, isomerization is hindered, and the state has non-reactive character. Last, similar to ^1Ag, the positive charge remains located on the $C=NH_2$ Schiff base end [83]. The different charge distributions in these three states lead to a situation where their energy differences, $\Delta E(S_1\text{-}S_0)$ and $\Delta E(S_2\text{-}S_1)$, are very sensitive to electrostatic interactions and thus to static or dynamic modifications of the environment (see below).

From recent quantum chemical computations, it is now well recognized that the energies of the ^1B_u and ^2A_g states are strongly dependent on the isomerization coordinate, hydrogen-out-of-plane motion and C=C dihedral angles, and that they may even come into degeneracy [84–88]. In such extreme cases, the $^1B_u/^2A_g$ mixing is complete, and the system oscillates in S_1 between the CT and DIR character, with a frequency determined by BLA. Such a regime was very recently reported to occur in bR, during the first 100 fs after excitation and only if the laser pulse was tuned to shorter wavelengths in order to explore higher vibronic states in S_1 [87].
In recent years, several papers reported on QM/MM calculations, which addressed the dynamic $^1B_u/^2A_g$ coupling along the reaction coordinate, in more general cases. Blending non-reactive ^2A_g character into the S_1 state, extends the excited state lifetime. It turns out that the strength of $^1B_u/^2A_g$ interaction depends critically on the GS geometry of the rPSB (e.g. 11-*cis* vs. all-trans) and on the electrostatic properties of the environment, no matter if it is a solvent or the protein cavity. The then created excited state potential energy landscape may be fully

reactive or present barriers (cf. **Error! Reference source not found.**-B), and is thereby determining the ESL and thus the FQY and isomerization reaction speed.

Since 13-*cis* rPSB in microbial protein environments have ESL close to the ones of 11-*cis* rhodopsin, and both types of chromophores are found to be non-planar, it was concluded that a pre-twist is synonymous of a displaced excited state potential [30,89–91] (in particular along hydrogen-out-of-plane motion (HOOP), which display larger Raman activities, cf. section III). This would lead to a more effective acceleration of the excited state wavepacket along the reaction coordinate [81,92]. Recent multi-configurational QM/MM simulations go a step further and rationalise the effect of the rPSB geometry on the excited state energy landscape computing the S_1 and S_2 energies of the full chromophore within CASSCF or CASPT2 approximations, and embedded in the respective natural protein environments (bovine rhodopsin for 11-*cis* – 11C/Rho; ASR for 13-*cis* (13C) and all-trans (AT), AMBER force fields)[86].

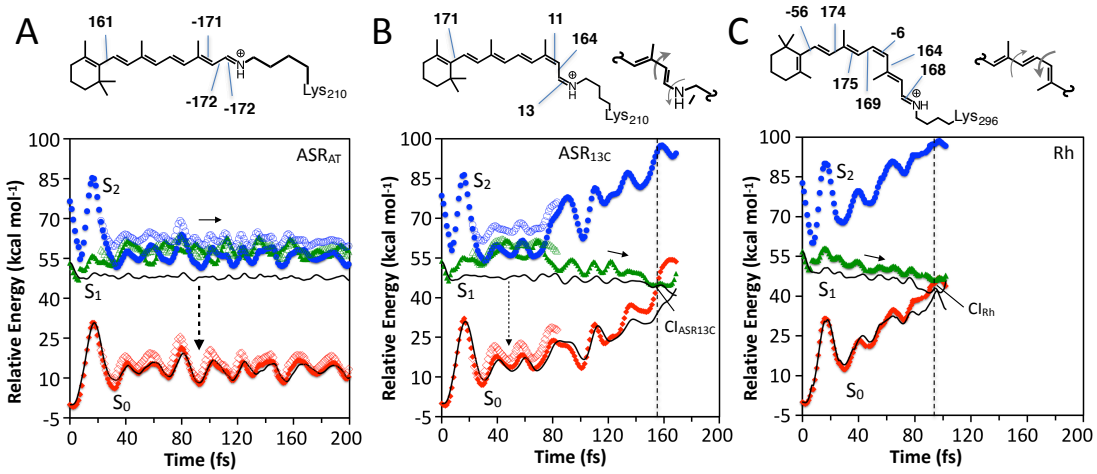

Figure 2: QM/MM trajectories of AT/ASR (A), 13C/ASR (B), and11C/ Rho (C). S_0 (red), S_1 (green), and S_2 (blue) The main out-of-plane (deviation larger than ±5°) dihedral angles of the S_0 equilibrium structure of the rPSBs are given at the top, together with the bicycle pedal motion driving the isomerization on S_1 with reversed bond order. The vertical dashed arrow represents weak fluorescence. Labels ASR_{AT}, ASR_{13C} and Rh correspond, respectively, to AT/ASR, 13C/ASR and 11C/Rho in the text. Reproduced with permission from [86].

Figure 2 shows the QM/MM trajectories for the three cases in the first 200 fs or until the S_1/S_0 CInt is reached. The computed energies are found to oscillate following the BLA. For 11C/Rho, S_1 and S_2 are separated at all times and they preserve their ^1B_u and ^2A_g character, respectively until the CInt is reached, i.e. the $^1B_u/^2A_g$ coupling is negligible (panel C). S_1 therefore preserves a strongly reactive CT character, and Figure 3 shows that bond length inversion is complete (BLA <0) along the C5=C6–C7=C8–C9=C10–C11=C12 fragment of the chromophore. Both effects lead in the specific protein environment to a barrierless potential and a rapid down-hill progression reaching the CInt within less than 100 fs, in agreement with experiments [31,93–96].

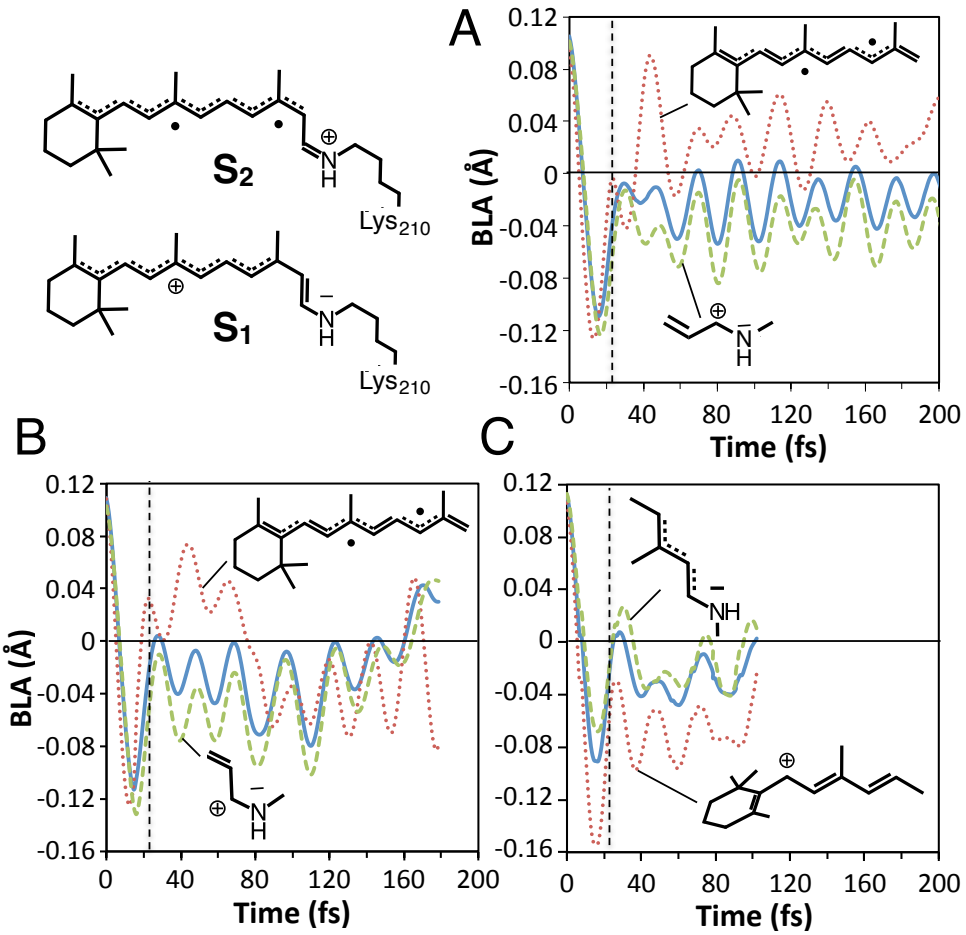

Figure 3: BLA changes in ASR and Rho. (A) BLA changes for the AT/ASR chromophore along the full conjugated chain (solid line), along the C5=C6– C7=C8-C9=C10–C11=C12–C13=C14 fragment (dotted line), and along the –C13=C14–C15=N fragment (dashed line). (B) Same data for the 13C/ASR chromophore. (C) The BLA along the full conjugated chain for the 11C/Rho (solid line), along the C5=C6–C7=C8–C9=C10–C11=C12 fragment (dotted line), and along the –C11=C12–C13=C14–C15=N fragment (dashed line). Reproduced with permission from [86].

In 13C/ASR, after an initial BLA displacement, S_1 and S_2 are degenerate in the 40-80 fs time interval, and the dihedral angles, along the C_{13}=C_{14} & C_{15}=N axes, remain almost planar [86]. During the same period, Figure 3 shows that BLA is positive, i.e. S_1 is dominated by a non-reactive DIR character associated with a very limited charge transfer from the -C=N moiety. Only after 80 fs, does S_1 display a negative BLA, a substantial charge transfer and a reactive ^1B_u character, with a down-hill progression towards the CInt by ≈150 fs, in agreement with experiments [19,90,97]. For AT/ASR, S_1 and S_2 are found to remain degenerate during the whole simulation interval of 200 fs (Figure 2). BLA is positive, meaning a non-reactive DIR character prevails (Figure 3-A), explaining the longer ESL observed for AT than for the 13C rPSB in ASR [19,90,97].

The above empirical rule stating that the chromophore's isomeric state combined with protein-imposed deformations would control the ESL can now be explained rather intuitively, in terms of the dominant ^2A_g or ^1B_u character. In fact, AT/ASR maintains four conjugated double bonds (C5=C6–C7=C8– C9=C10–C11=C12–) with a reduced, but still positive BLA, rather than bond length inversion (Figure 3-A). Such a polyene-like pattern accommodates the non-reactive DIR electronic structure better than the CT structure. On the other hand, due to the pre-twisted β-ionone ring on one side and the rapidly twisting C11=C12 on the other,

11C/Rho offers a shorter fragment with two conjugated double bonds (C7=C8–C9=C10–C11) with a negative (inverted) average BLA value (Figure 3-C). As a consequence, $\Delta E(S_2\text{-}S_1)$ will rapidly decrease towards a degeneracy along the photoisomerization coordinate in AT/ASR and 13C/ASR but not in Rho.

In subsequent publications, the concept of $^1B_u/^2A_g$ mixing was further investigated computationally for the environment-induced differences of 11-*cis* rPSB in methanol and in Rho [84], and for the effects of substitutions of the all-trans rPSB in solution with electron-donating or –withdrawing groups [84,88]. Experimental data, regarding the ESL [11,98], where consistently reproduced and explained in terms of the build-up of an excited state barrier or flat, population-stabilising regions due to an increased ^2A_g character in the S_1 state, limiting its reactivity. In summary, the concept, which emerges from these theoretical results, is that both steric and electrostatic effects act through the modifications of the S_1/S_2 energy landscape in determining the ESL of rPSB in different protein environments (exemplified in detail in chapter III), and also of rhodopsin-mimicking photo-switches in solution (chapter IV).

III. Effects of point mutations: the case of Anabaena Sensory Rhodopsin

Anabaena Sensory Rhodopsin (ASR) is a membrane protein of 261 residues (26 kDa) found in the eubacterium *Anabaena* (Nostoc) sp. PCC7120 [99], and is part of the family of archeal microbial rhodopsin, as much as bR or sensory rhodopsin from *Halobacterium salinarum [1,100].* The main structural differences with respect to bR are the replacement of Asp212 in bR by Pro206, a non-polar residue, in the vicinity of the rPSB and a hydrogen-bonding network from Lys210 to Glu36 [101].

Regarding the ultrafast photo-isomerization, it is most notable that ASR bears a mixture of all-trans,15-anti (AT) and 13-cis, 15-syn (13C) rPSB isomers, the relative content of which depends on the illumination, so-called 'light-adaptation' conditions. When left in the dark, the dark-adapted (DA) form adopts 97% AT, which drops to less than 50% under illumination with orange light, at neutral pH [102]. In the context of obtaining insight into the mechanisms by which retinal proteins catalyze the rPSB photo-isomerization reaction, ASR is a model system allowing to study, within the same protein, the protein–rPSB interactions for two different rPSB conformers at the same time. Interestingly, at pH=7, both isomers display markedly different excited state lifetimes (ESL): ~0.7 ps for AT, and approx. 150 fs for 13C [19,90,97,103]. This was empirically related to the fact that 13C is twisted in the ground state conformation [101], but different electrostatic or dynamic interactions with the protein charge distribution may also play a role. The different excited state lifetimes were rationalized by quantum chemistry computations of the excited state potential energy surface (PES) along the minimum energy paths in ASR [22], and with excited state trajectory calculation [84,86,104]. As shown in Figure 2, it was found that the S_1 PES of 13C is barrierless, while that of the AT form displays a plateau or a slight barrier that could account for a short resting period of the excited state population. The precise origin of these different shapes of the S_1 PES for both isomers, and the mechanism of their fine-tuning by the protein interaction has motivated the research efforts described below. While sections *a* and *b* summarize primarily experimental work on the electronic and vibrational dynamics of AT and 13C/ASR, as a function of mutations, section *c* reviews a combined experimental/theoretical study of two cases of mutations which track the molecular origin of a 12-fold enhancement of the ESL.

a. Effect of mutations on the ESL: Rationalising spectral shifts and effects on excited state lifetimes

Our first joint paper on mutation-induced effect in ASR, published in 2018, reported a combined experimental and computational study of the spectral shifts, the ground state vibrational spectra and isomerization reaction times of the AT and 13C isomers in the mutants L83Q, V112N and W76F [105].

Effects of the modified protein electrostatics on the isomer-specific absorption spectra. In L83Q and V112N, the nonpolar residues Valine and Leucine are replaced by the polar but neutral Glutamine (Q) and Asparagine (N), respectively, while the W76F mutation reduces the electron density and removes a small dipole close to the rPSB backbone (Figure 4). All mutations lead to blue-shifts of the DA and LA ground state absorption spectra with respect to wt-ASR [105]. Light- adaptation was carried out either with an orange (OA, 590 nm) or a blue (BA, 460nm) LED, and the light-adaptation with the highest 13C isomer ratio was retained. The latter was higher than 50% in all cases, as for wt-ASR. V112N and W76F exhibit a blue-shift under LA as wt-ASR and many other mutants. The absorption spectrum of the 13C isomer of these mutants shifts by 2 nm (V112N) and 8 nm (W76F). L83Q, the blue-most shifted mutant, surprisingly shows the opposite effect, with the 13C isomer being 6 nm red-shifted with respect to AT.

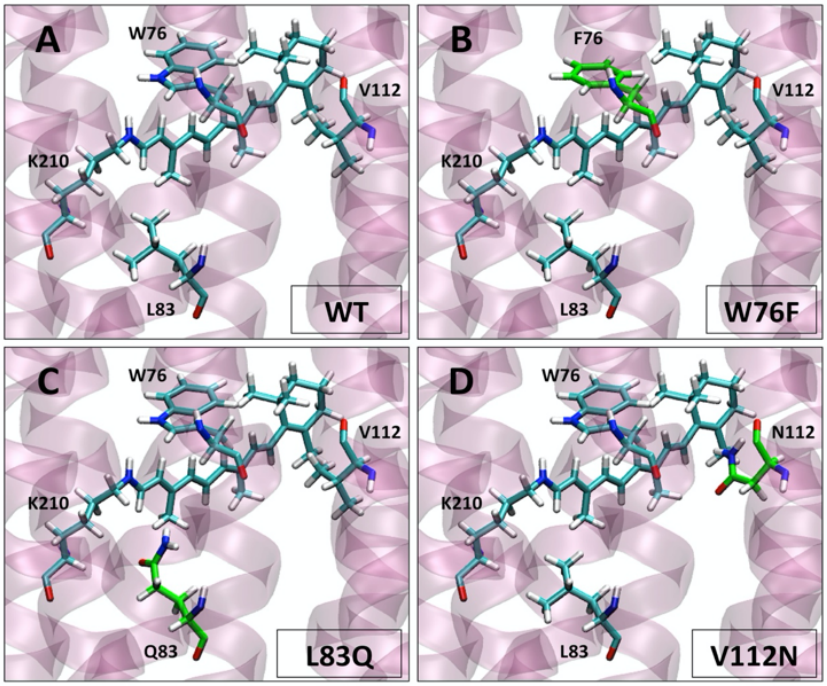

Figure 4: Calculated structures of the AT rPSB and the mutated residues L83, W76 and V112N in DA ASR (A). The replacement of Trp76 by a Phenylalanine reduces the electron density close to the AT rPSB backbone (B). Introduction of the polar Glu at position 83 and Asp at position 112 (C&D) changes the electrostatic interactions with rPSB in both S_0 and S_1.

From a purely computational structure of the mutated protein-chromophore complexes, obtained by the automatic retinal protein model (ARM) [106], the mutation-induced shifts were correctly reproduced, as well as the amount of LA-induced blue-shifts for W76F and V112N. For L83Q, ARM produced a wrong orientation of the dipoles of Q83, which was corrected "manually". This produced absorption maxima consistent with the observations, including the inverted LA effect. By comparing both the effects of steric and electrostatic modifications, it was concluded that the latter effects are dominant, in particular for W76F. Indeed, the mutation-induced changes of the rPSB configurations cause, with respect to the wt-ASR, rather a red-shift and not the experimentally observed blue-shifts. For both the V112N and W76F mutants, a change from Valine to Asparagine, near the ionone ring of the

chromophore, and Tryptophan to Phenylalanine produces a destabilization of S_1 and a smaller stabilization of S_0. Hence, the observed blue-shift of the S_0-S_1 transition energy is a combined effect of S_1 up-shift and S_0 down-shift.

Effects of the modified protein electrostatics on the reaction kinetics. The excited state lifetimes and the isomerization reaction times were determined by broadband transient absorption spectroscopy in the 340-750 nm range, covering the characteristic bands of ground state bleach (GSB), excited state absorption (ESA) and stimulated emission(SE), as well the photo-product absorption in the J and K states of both AT and 13C isomers. The latter are obtained by the standard procedure subtracting the experimentally determined contribution of AT excited isomers, from the LA data. Values for ESL were extracted from ESA and SE decay times. For the AT isomers (DA), the ESA decay appeared to be bi-exponential, while it displayed mono-exponential decays for the small signal SE region probed (700-750nm). When the SE is studied at longer wavelengths and maximum signal, all mutants display a multi-exponential excited state decay, as found for wt-ASR [90], and in agreement with the ESA decays (to be published). The fast component was found to be significantly reduced with respect to the 0.75 ps ESL of AT in wt-ASR, with L83Q showing an ESL as short as 120 fs. Whether the second slower component (in the 0.5-0.7 ps range, amplitude ≤30%) also leads to isomerization is difficult to ascertain since the rise of the photo-product (PPA) or J-state absorption naturally allows to unambiguously determine only the fastest component. A potential slower rise appears to be rather compensated by the signal decay to the J-to-K vibrational relaxation (Figure 5). We therefore quoted the "isomerization reaction time" (IRT) extracted from a combined analysis of GSB, ESA, SE and PPA: L83Q - 120 fs, V112N – 230 fs and W76F 340 fs for the AT isomers. These values are presently reconsidered on the basis of the near-IR SE, which allow to determine ESL with higher accuracy (higher signal and zero background, Figure 5). Nevertheless, the initially reported incidental correlation is confirmed: the larger the spectral blue-shift of the GSA, the smaller the IRT.

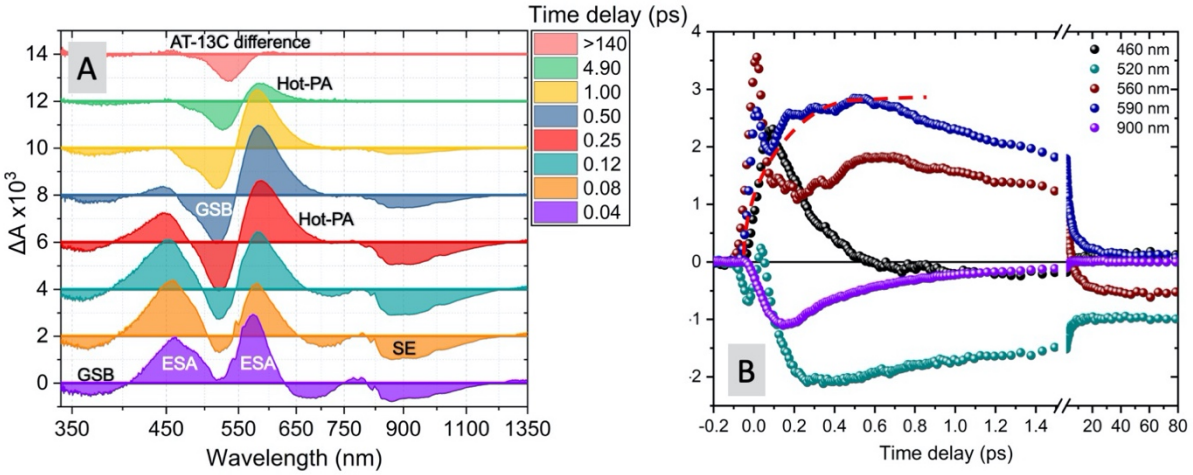

Figure 5: Transient absorption data for the ASR mutant L83Q in DA conditions (≈100% AT). (A) : Combined UV-VIS and near-IR prob wavelengths, for the delay times indicated in the legend. Ground state bleach (GSB), excited state absorption (ESA), and stimulated emission (SE) highlight signal from S_1. In the 550-600 nm range ESA turns into "hot" ground state absorption by ≈200 fs. (B) Kinetics at selected wavelengths. The red dashed line is a guide to the eye with a 200 fs rise time for the "hot" ground state absorption.

For 13C, the mutations did not alter the IRT as much as for AT, but the values rather indicate the opposite trend: a small but significant increase of ESL and IRT. This an important result, which confirms the initial strategy of choosing ASR as a model system: the protein-chromophore interactions act differently, namely in an opposite fashion, on the two isomer

conformations. The molecular basis for this observation is unclear and is the subject on ongoing work both computationally and experimentally. A central question is to figure out in as much LA changes the entire coupled protein-chromophore system in what we call the "13-*cis* isomer". i.e. both the chromophore and the protein likely undergo LA-induced structural changes.

b. Details from femtosecond vibrational spectroscopy

First vibrational spectra obtained by femtosecond non-resonant (pump-)DFWM were also reported in this paper [105] for the isomer ground states in DA and LA, as well as their photo-isomerized K states (pump delay 100 ps). The procedure for extracting AT- and 13C-pure vibrational spectra was explained in detail, and exploited more thoroughly in a subsequent publication [91], summarised and discussed in the following.

The vibrational spectra of both AT and 13C isomers in ASR both in the ground and excited states were analysed in detail [91]. The experimental techniques used rely on degenerate four-wave-mixing (DFWM) and impulsive vibrational spectroscopy (IVS), which can be performed also in the excited state, due to the action of an actinic pump pulse as a function of delay time [107–110].

The ground state vibrational spectra of both DA and LA forms of ASR were obtained by non-resonant DFWM and IVS, and compared to traditional spontaneous Raman spectra. Non-resonant schemes used a spectrally broad sub-15fs pulse centered at 650-660 nm, and revealed very different resonances in the high-frequency range above 1000 cm^{-1} and, most importantly, a much stronger Raman activity for 13C in the hydrogen-out-of-plane (HOOP) region around 800-900 cm^{-1}. All these observations are in-line with the differences between AT and cis rPSB conformations in other retinal proteins, like bR or channel-rhodopsin. Supported by MD simulations on the ground state, it was suggested that the larger distortion hinted on by the HOOP activity is located at the C14-C15 bond, rather than on the reactive C13=C14 bond, in agreement with X-ray data of ASR [101]. As for 11-*cis* rPSB in Rho, this pre-twist of the 13C chromophore, as opposed to the planar AT configuration, was identified as one of the reasons for the shorter ESL of 13C.

The structural changes in the excited state were followed by exciting each isomer with an actinic pump. The pure spectra of the excited state was obtained since the GS spectra of each isomer and the photo-products K_{AT} and K_{13C} could be measured separately [91]. In particular, the frequency of the C=C stretch and CH_3 rocking modes showed a transient blue-shift for both isomers, consistent with a reduced conjugation length, induced by the torsional motion. Indeed, in a 90° twisted conformation, the C14–C15–N and C5=C13 moieties are disconnected electronically. Most importantly the dynamics of the transient frequency shifts mirrors the excited state and reaction lifetimes qualitatively. The blue-shift occurs almost immediately upon excitation for 13C and decays with a half-time of 150 fs. The AT frequency shifts reach maximum only after 0.2 ps and adopt the K_{AT} values only by 0.6 ps. These studies also showed that the amplitude of these isomerization-induced changes in the CH_3 rock frequencies were different for AT as for 13C, which is taken as an indication that isomerization causes a larger rotation around the central C13=C14 bond for AT than for 13C, in agreement with previous FTIR results on the cryo-trapped K intermediates [102].

In addition, low frequency vibrations (< 400 cm^{-1}), related to excited state modes, identified previously in transient absorption experiments [97], were shown to appear after a short induction time; shorter for 13C than for AT.

Effects of mutations on the ground state vibrational spectra. The mutants L83Q and V112N were studied by femtosecond DFWM and IVS in the DA and LA states [111], under exactly the same conditions as the ones used in the above TA experiments. It was found that mutations lead to an enhanced HOOP mode activity in the AT ground state of L83Q and V112N indicating a pre-distorsion of the chromophore either around the active C13=C14 bond or neighbouring C14−C15 bond of the ground state compared to the AT-isomer in the wt-ASR [111]. Additionally, the high frequency vibrations related to C-C single bond or C=C double bond stretch, as well as CH_3 rock modes change consistently with a reduced conjugation length, induced by the pre-distortion. In agreement with previous experimental and theoretical work, the pre-distortion is held responsible for the drastic reduction of the excited state lifetimes for the mutants, as compared to AT in wt-ASR. On the other hand, the mutations do not seem to enhance the pre-distortion already observed for the 13C isomer in wt-ASR, in agreement with a small increase of the ESL for 13C.

In summary, time-resolved vibrational spectroscopy, here accessed via degenerate FWM and IVS, provided new insights on structural changes during the isomerization process. For wild-type ASR and its mutants, the observations are perfectly in line with the theoretical predictions outlined in chapter II (Figure 2), underlining here the role of a pre-twist in 13C/ASR for reducing the excited state barrier and leading to the shorter ESL.

c. Towards a rational prediction of the excited state lifetime of AT rPSB in mutants

While a detailed and comprehensive computational analysis of the mutation-induced effects on the excited state lifetimes of AT and 13C for the above mutants is still ongoing, we examined further mutations with the aim of achieving an ASR mutant with an increased excited state lifetime and thus FQY. This is of particular importance in the area of optogenetics, combined, if possible, with an increased absorption of the mutants in the red or near-IR region of the spectrum [24]. We recently reported an almost 10-fold increase of FQY in the ASR double mutant W76S/Y179F, and rationalised the observations within the context of the modified protein electrostatic environment, including the computational analysis of the excited state electronic structure and lifetimes of wt-ASR and the L83Q mutant [112]. The theoretical framework outlined in section II, is central to understanding the mutation-induced modifications of the $^1B_u/^2A_g$ mixing along the reaction coordinate, which, in this paper was traced down to the electrostatic interactions of the mutated residues.

The experiments were performed on the DA forms of wt-ASR and on the L83Q and W76S/Y179F mutants, together with two light-adapted forms of the latter. We focused on the mutation effects on the AT isomers, which accumulates to > 95% in DA wt-ASR and L83Q, and is highest in orange-adapted form of W76S/Y179F (39%). While fluorescence of the non-canonical 7- and 9-*cis* isomers was minimised in the double mutant, by excitation with > 520 nm light, contributions from 11- and 13-*cis* cannot be excluded. We found that the FQY was lowest for wt-ASR and increased by a factor of 2.2 for L83Q, and by 7.9 and 6.9 for orange- and green-adapted W76S/Y179F, respectively.

The mutation-induced shifts of the ground state absorption and steady-state emission spectra are reported and reproduced with high accuracy by the QM/MM method. The latter is based on the ARM protocol [113], which employs the CASSCF method which is an ab initio (wavefunction-based) multi-configurational quantum chemical (MCQC) method coupled with the Amber molecular mechanics force field to obtain the S_0 QM/MM models of rhodopsins semi-automatically. Vertical excitation energies are then computed using multiconfigurational second-order perturbation theory (CASPT2) to account for the missing dynamic electron correlations. The level of agreement with the observed trends in absorption and fluorescence experiments indicate that the descriptions of the steric and

electrostatic effects of the different protein environments on the S_0 and S_1 relaxed structure are trustful, and can be extended to describing the S_1 dynamics.

These were experimentally probed by measuring the decay of stimulated emission (SE) in the 850-1250 nm range, with ≈60 fs time resolution. The SE decays turned out to be almost wavelength-independent, and bi-phasic for all studied ASR variants. We thus compared the average values of ESL with the relative increase of FQY, and found that the FQY increases proportionally to ESL for W76S/Y179F with respect to wt-ASR, according to $FQY = ESL \times k_r$ with k_r the radiative rate, generally assumed to be constant. Interestingly, L83Q showed a 2.2-times larger FQY than wt-ASR, despite an almost 2-fold reduction of the ESL, indicating that L83Q has a higher radiative rate than the wild-type. This and the effects of the mutations on ESL were explained by calculations of the S_1 relaxation/reaction paths and by computing 200 fs semi-classical trajectories (Figure 6).

Indeed, relaxed scans of the S_0, S_1 and S_2 energies along the C12−C13=C14−C15 dihedral angle, computing minimised energies for fixed dihedral angles, indicate that the S_1 profile is barrierless for L83Q, while it is flatter and displays shallow barriers of ca. 3 and 6 kcal/mol for wt-ASR and the double mutant, respectively. The barriers have a maximum close to 120° torsion of the reactive C13=C12 double bond. The excited state lifetimes are best simulated by trajectories computing the time-dependent energies of the S_1 and S_2 states and their crossing with S_0 at a conical intersection (Figure 6). Here the kinetic energies in all vibrational modes of the chromophore are included, leading to different and time-dependent energy differences, in particular between S_1 and S_2. Only for L83Q do the computations predict an ultrafast S_1/S_0 crossing by ≈100fs, consistent with the fastest 0.27 ps decay time observed in SE. On the other hand, Figure 6 shows that wt-ASR and W76S/Y179F do not reach the CI within the simulation time, consistent with the observed shortest decay times above 500 fs and with the computed S_1 barriers in the relaxed energy scans.

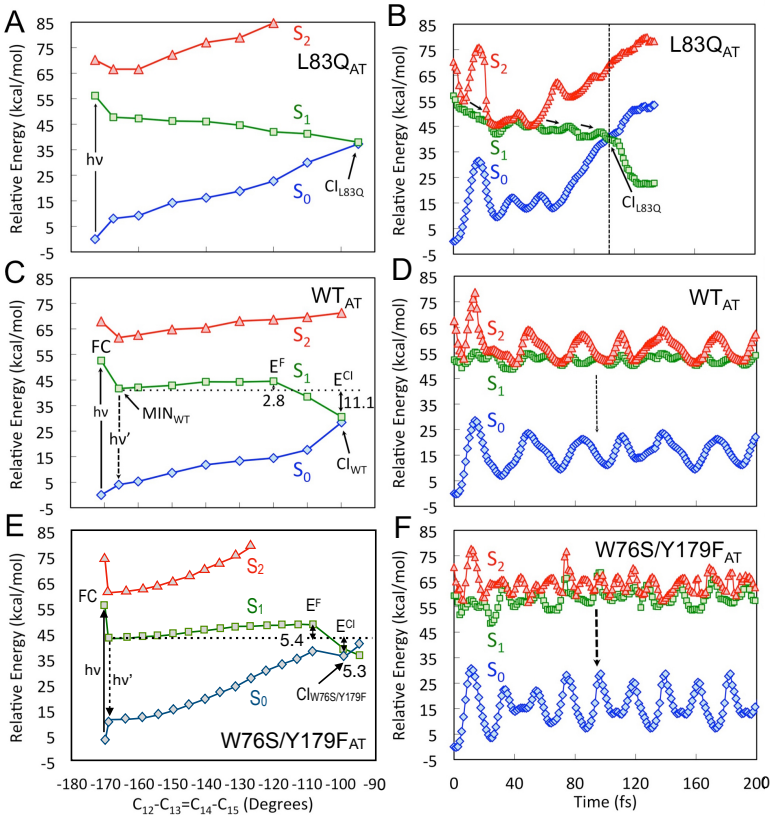

Figure 6: (A,C,E): CASPT2// CASSCF/AMBER energy profiles along the S_1 (green squares) isomerization path of L83Q, wt-ASR, and W76S/Y179F, respectively, computed in terms of a relaxed scan along the C12−C13=C14−C15 dihedral angle. Note the appearance of an excited state barrier for wt-ASR, and W76S/Y179F. Energy profiles of S_0 and S_2 are indicated by blue diamonds and red triangles, respectively. (B,D,F): Excited state QM/MM FC trajectories of L83Q, wt-ASR, and W76S/Y179F, computed at three-root state-averaged-CASSCF/AMBER level of theory and corrected at the CASPT2 level. S_0 (blue diamonds), S_1 (green squares), and S_2 (red triangles) CASPT2/CASSCF/AMBER energy profiles along the FC trajectories. The reaction path diagram in panel E is different from the corresponding panel in ref. 112. In fact, the presented path has been computed using a 3-root CASSCF level - rather than 2-root state average - to be consistent with the results presented in panels A and C.

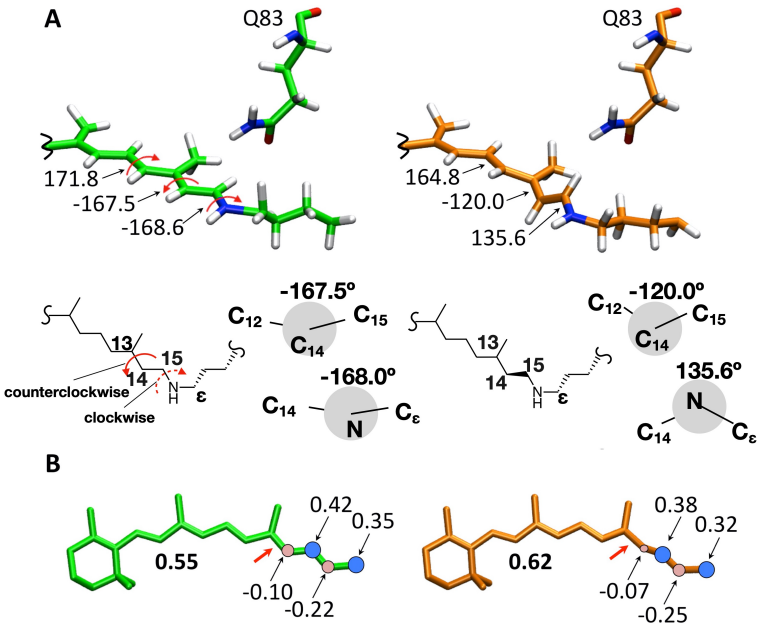

Figure 7: Evolution of the dihedral angles (A) and charges on the Schiff base end (B) along the isomerization path for L83Q. The C12−C13=C14−C15 dihedral angle is ≈-170° (left) and -120° (left). Adapted from ref. [112].

Interestingly, the mutations act through different mechanisms on the $^1B_u/^2A_g$ mixing. For L83Q, the reactive character of S_1 is induced through electrostatic interactions imposed by the protein environment, while in W76S/Y179F the stabilisation of emissive regions on S_1 is due to subtle changes of the chromophore structure. This was given evidence for by computing the S_1 energy profiles along the isomerization paths in *vacuo*, i.e. for the isolated rPSB taken with its protein geometry. Indeed, in the case of the L83Q chromophore structure, the energy profile appears to be very similar to the one detected for the rPSB in wt-ASR and W76S/Y179F protein environment, which would lead to a picosecond excited state lifetime and an enhanced emission. Since these are not observed, the short ESL in L83Q is a consequence of the protein environment. The computations indicate a reorientation of the π-conjugated chain along the reaction path in a way that enhances the interaction with the polar side chains of Q83. At the same time, the positive charge on the Schiff base end is further reduced upon increasing the C12−C13=C14−C15 dihedral angle (Figure 7). Both effects lead to an electrostatic stabilisation of S_1 along the reaction paths and thus to a barrierless progression on the S_1 PES.

On the other hand, the *in vacuo* analysis for wt-ASR and W76S/Y179F shows no qualitative changes in the energy profiles with respect to the respective protein environments. This indicates that the S_1 barrier is not induced but only marginally modulated by electrostatic interaction. Rather, it is an intrinsic feature of the rPSB conformation. The increased S_1 barrier in W76S/Y179F is due to subtle geometrical changes with respect to the rPSB geometry in wt-ASR. Indeed, the computations show that it is possible to transform the wt-ASR S_2, S_1, and S_0 energy profiles into W76S/Y179F-like energy profiles by simply changing the backbone dihedral angles along the wt-ASR reaction coordinate to the corresponding W76S/Y179F values. This is remarkable because those are limited changes that indicate

the fluorescent tuning in rhodopsins might be achieved also through subtle geometrical (i.e. steric) effects.

In conclusion, this combined experimental and computational study outlines two pathways for a rational design of ASR mutants with enhanced ESL and FQY. It was shown that mutations can induce steric effects that induce a pronounced $^1B_u/^2A_g$ mixing, blending non-reactive character into S_1 through geometrical effects. Alternatively, it might be interesting to engineer the mutations such that the dynamic electrostatic interactions with the increasing CT character of the rPSB are of repulsive character so as to destabilise S_1 and maintain a significant $^1B_u/^2A_g$ mixing.

IV. Retinal-inspired molecular switches: towards controlling photoreactivity by synthetic chemical design

An alternative, complementary strategy to decipher the tuning mechanism of the rPSB photoreactivity in rhodopsins has been to design a model chromophore that mimics – in solution - the electronic structure, PES topologies and eventually photoreactivity of 11-*cis* rPSB in the visual pigment of Rhodospin (Rho) [114,115]. In Rho, the photoisomerization is remarkably fast (<200 fs) and efficient (isomerization quantum yield, IQY = 67%) [93,94]. Above all, this photoreaction is vibrationally coherent, a unique mechanism enabling to funnel the energy of the absorbed photon specifically into the isomerization coordinate on a time scale faster than vibrational dephasing, and held responsible for the enhanced IQY in Rho[23]. Revealing the chemical design principles underlying such an efficient light to mechanical energy transduction at the molecular scale would be of central interest in the prospect of designing efficient molecular switches and motors [116].

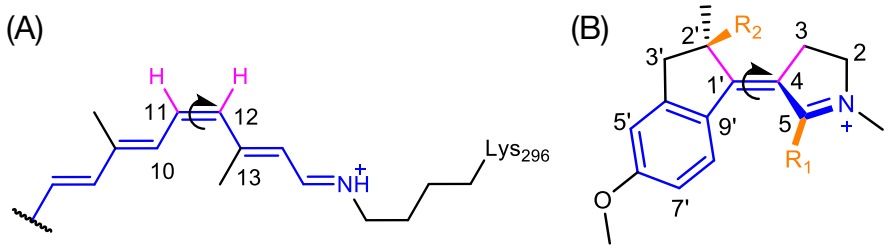

Figure 8: Chemical structure of (A) the 11-cis isomer of rPSB in Rho, and (B) the Z isomer of the IP compounds. Both IP and rPSB have a similar π-electron system (blue molecular backbones) with an S_1 state characterized by a bond length alternation and partial reduction of the protonated Schiff base through charge transfer along the carbon backbone. They also have an analogous photoreaction coordinate, which involves the torsion around the central C=C double bond (curved arrows) as well as out-of-plane motions of the purple bonds. Several IP compounds have been synthesized and studied theoretically and experimentally. They differ by the substitutions in orange: R1 = H or Me, R2 = H or Me.

As discussed above in the case of ASR and due to the CT character of the S_1 state, a major parameter influencing the photophysical properties of rPSB is the protein electrostatic environment and the counterion neutralizing its positive charge [56,117]. In the originally proposed N-alkylated IP compounds – which we name MeO-NAIP - the electron-donating MeO group on C6' stabilizes the S_1 state by favoring its CT character, thus mimicking the stabilizing effect of the electrostatic protein environment in Rho [114]. Besides fine-tuning the S_1 CT character, another central ingredient of the biomimetic design is the intramolecular steric hindrance imposed by the two methyl groups on C2' and the methyl group on C5. Altogether they impose the *Z* configuration of the MeO-NAIP to be the most stable S_0 isomer, in a non-planar - pre-twisted – geometry. Recently, we revealed the effect of the Me substituent on C5 on the IP photoreactivity by investigating the "demethylated" MeO-NAIP

compound, named dMe-MeO-NAIP, which features no methyl on C5 (R1=H in Figure 8). As we will illustrate below, we demonstrated that while the parent MeO-NAIP undergoes a vibrationally coherent photoreaction mimicking that of rPSB in Rho, this is not the case of dMe-MeO-NAIP. In a way similar to the case of rPSB in retinal proteins and mutants, we could conclude that this difference in photoreactivities observed within the two IP compounds is closely related to the S_1-S_2 energy gap and mixing, itself controlled by electrostatic and (intramolecular) steric properties.

UV-Vis or mid-IR transient absorption (TA) spectroscopy as well as femtosecond fluorescence spectroscopy were used to investigate the ultrafast photoisomerization reaction of a variety of IP compounds in solution [20,115,118–122]. While all compounds undergo a subpicosecond photoisomerization, they can be categorized within two photoisomerization scenarios, corresponding to two qualitatively distinct spectroscopic signatures, as illustrated in Figure 9. For the so-called "parent" NAIP compound [121] and its zwitterionic derivative [119], the excited state absorption (ESA) and stimulated emission (SE) from the S_1 population (Figure 9 a) are very short-lived, they spectrally shift to the blue and to the red respectively, and they decay impulsively by 250 fs (vertical dashed line across Figure 9 a,c,e). The ground state photoproduct absorption (PA) band immediately follows, which initially appears after the decay of the SE in the low-energy spectral range (600-700nm), and rapidly blue shifts to ~430nm within ~0.5ps. Such dynamic spectral shifts of the S_1 and early S_0 bands have been interpreted as the signatures of a population which evolves ballistically from the FC region to the photoproduct ground state through the Cint in the form of a vibrational wavepacket [119]. A very similar red-shifting SE impulsively followed by a blue shifting PA has been reported in Rhodopsin too and interpreted the same way [94]. Further evolution in the ground state is accompanied by a pronounced low-frequency oscillation (~80 cm^{-1}, corresponding to ~500 fs period, Figure 9 e) interpreted as the signature of a vibrational wavepacket oscillating around the S_0 PES minimum along the C=C torsion coordinate [119,121]. Importantly this vibrational wavepacket was demonstrated to be triggered by the S_1 reactive motion, meaning that this low-frequency vibrational coherence is preserved through the CInt and exponentially damped (with a ~300 fs time constant) after the decay to S_0 [118].

Conversely, the "demethylated" NAIP compound, where C_5 carries an H atom in place of a methyl substituent, has a very similar ground state spectrum but qualitatively different TA signatures (see Figure 9 b,d,f): The SE signature does not extent this far to the low-energy range, it is spectrally narrower and longer-lived. The SE and ESA bands decay in concert with the rise of the PA band which appears gradually at 430 nm, rather than impulsively in red part of the probing window. Hence there is no similar indication of a vibrationally coherent reactive motion that would impulsively drive the system through the CInt as discussed above. More precisely, upon light excitation with a very short (8fs) pump pulse, a vibrationally coherent motion is detected in S_1 along (in particular 232 cm^{-1} mode, see Figure 9 f). However, no vibrational coherence is transferred to the ground state, and in particular no vibrational activity is detected at 80 cm^{-1}.

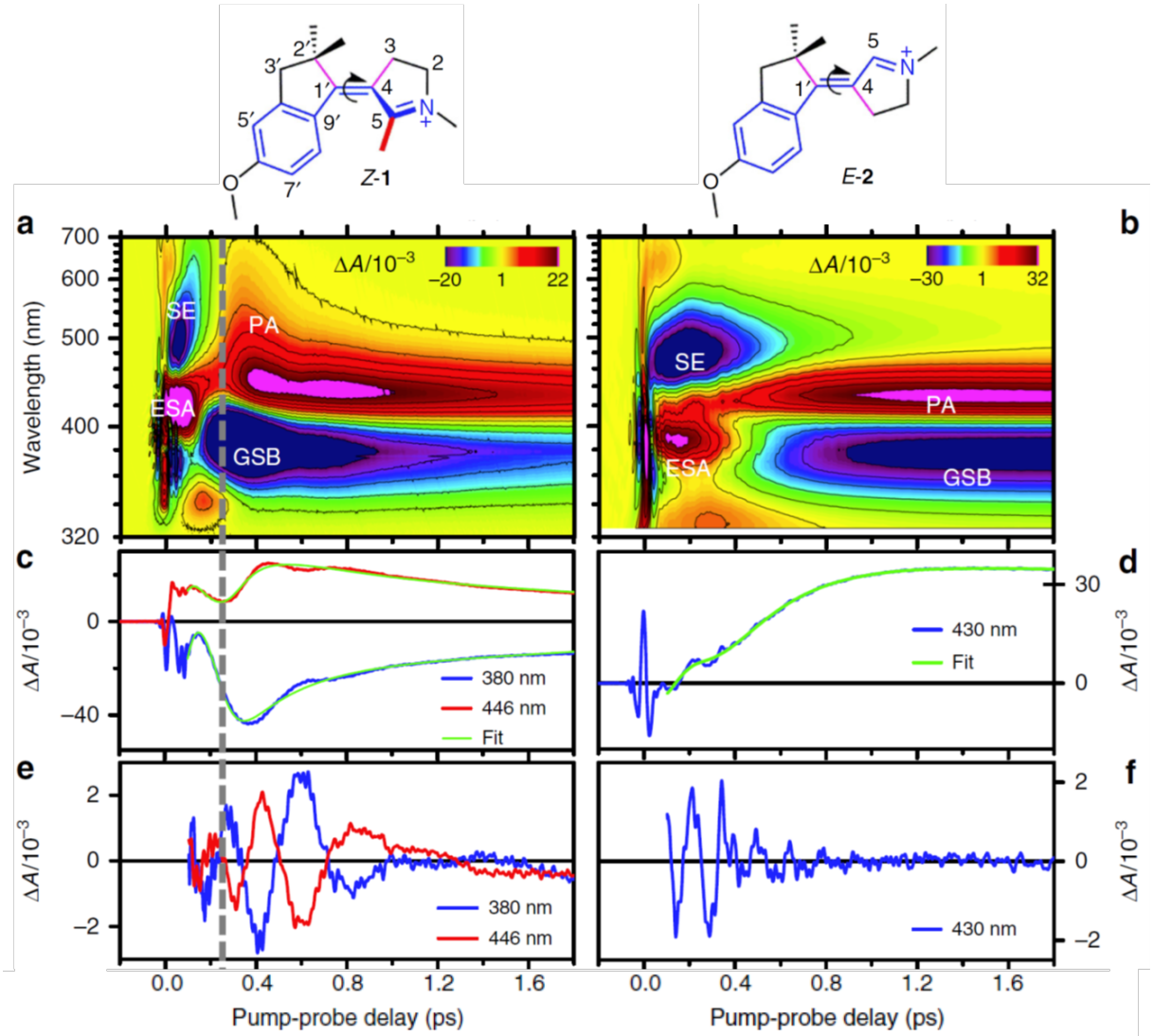

Figure 9: Transient absorption spectroscopy (TAS) of two representatives of the NAIP compounds family obtained with an 8-fs, 400-nm pump pulse. Compound Z-1 carries a methyl in C5 and its C=C double bond is pre-twisted in S_0. Its TAS signatures (a) are qualitatively different from those of the "demethylated", planar compound E-2 (b) where the methyl group on C5 is replaced by a H atom. (c, d) Selection of transient kinetics traces from the above datasets, and their fits. (e, f) The residuals of the fits are oscillatory signals revealing the vibrational dynamics accompanying the photoreaction. Abbreviations: GSB = Ground State Bleach; SE = Stimulated Emission; ESA = Excited State Absorption; PA= Photoproduct Absorption. Reproduced with permission from [118].

To rationalize why these two compounds undergo such qualitatively different photoreactions, we first notice, that the most stable ground state isomer is *Z*, with a ~15° pretwisted C=C bond, for the C5-methylated compound, but *E* in a planar conformation for the demethylated compound. These differences are controlled by the intramolecular steric hindrance introduced with the methyl substituent on C_5, which also affects the S_1 electronic structure and photoreactivity of the compounds, as rationalized by QM/MM modeling at the CASSCF/CASSPT2 level [118]. Indeed, in the planar compound, the S_1 and S_2 states are computed to be nearly degenerate, resulting in a flat S_1 PES, while in the pre-twisted compound the degeneracy is lifted and the S_1 PES slope is very steep. Consequently, in the latter case, the motion along the torsion coordinate is strongly accelerated which drives the system ballistically towards the CInt, such that the photoproduct formation occurs faster than vibrational decoherence of the 80 cm^{-1} mode, resulting in the pronounced oscillatory signal observed after the decay to S_0. In the former case, a more diffusive exploration of the S_1 PES potential would be responsible for an increased excited state lifetime and vibrational

decoherence would be effective already by the time the system reaches the CInt and decays to S_0 (Figure 10).

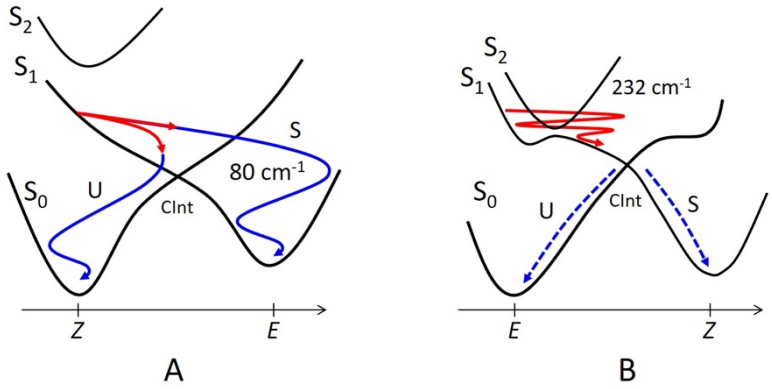

Figure 10: ***Schematic representations of the two distinct photoisomerization scenarios in the NAIP compounds.*** *(a) The reactive motion of the pretwisted MeO-NAIP is governed by a steep S_1 PES driving the system ballistically towards the CInt. Upon impulsive decay to S_0, this S_1 motion coherently populates the S_0 vibrational motion along the torsion mode at 80 cm^{-1}. (b) Instead, for the planar demethylated compound, the S_1 and S_2 states are nearly degenerate, resulting in a flat PES providing a much weaker acceleration along the torsion mode, and a more diffusive motion towards the CInt. The crossing of S_1 and S_2 leads in fact to an avoided crossing. The corresponding loss of synchronization then explains the observed loss of ensemble coherence. Two decay channels ("U"="unsuccessful", and "S"="successful") are represented, with the evolutions on the S_1 or S_0 PES represented in red and blue, respectively. The 20 to 25% quantum yield indicates that channel U is dominating. Adapted from [118].*

By comparing the TA signatures and photoreaction scenarios for each isomer of half a dozen of NAIP derivatives [20], we observe that all compounds under investigation obey either the first or the second photoreaction scenario. Moreover, based on DFT modeling of the compounds S_0 equilibrium structures, we establish a perfect correlation between the C=C double pre-twist and the photoreaction scenario: All compounds featuring a significant (>10°) pre-twist obey the first photoreaction scenario, and all compounds featuring a more planar S_0 conformation (<10° pre-twist) obey the second one. This allows us to generalize the central role of the intramolecular steric effect and pre-twist at controlling the PES topography via the fine tuning of the S_1-S_2 state mixing in these retinal-inspired compounds. As reviewed in chapter II&III, the same effect of a pre-twist of the chromophore is operative in 13C/ASR in reducing the excited state barrier [111].

A major outcome of our latest study [20], is that while the intramolecular steric hindrance and related S_1-S_2 state mixing controls the photoreaction dynamics, we observe no correlation between the IQY – in the range 15 % to 35 % for all IP compounds investigated – and observables such as excited state life time, vibrational coherence, absorption wavelengths or degree of pre-twisting. The molecular mechanism controlling the IQY in ultrafast C=C double bound isomerization thus remains an open question so far.

V. Summary and conclusions

In summary, for the sub-picosecond isomerization reactions of rPSB in a protein cavity and for the related bio-mimetic switches in solution, modifications of the ESL can be induced by steric effects (ground state pre-twist) and by changes in the electrostatic environment. The experimental and theoretical studies on the AT and 13C isomers ASR and its mutants have identified both effects, and how they are brought about by point mutations. For the photoswitches, steric [118] and electronic [20,123] effects, brought about by substitutions of the NAIP framework were investigated experimentally. These studies showed, in addition to

the change in ESL, a clear influence on the survival of vibrational coherences in the ground state. The computational framework shows that both steric and electrostatic parameters affect the excited state structure due to $^1B_u/^2A_g$ mixing, and how it determines the CT and reactive character in terms of BLA of the lowest excited state S_1. A central point is that the simulations allow to predict how this mixing changes dynamically when the chromophores evolve along the reaction coordinate. Shallow excited state barriers appear when S_1 alternates between a reactive CT and non-reactive DIR character, leading to longer ESL and higher FQY. The recent experimental observation of BLA-mediated $^1B_u/^2A_g$ oscillations demonstrates this effect clearly, within the first 100 fs of the excited state reaction in bR [87].

In order to obtain a more direct experimental insight, and a direct comparison with the simulations, measuring the time-dependent S_1-S_2 splitting would provide new insights for systems with reactive vs. non-reactive excited state dynamics. The S_1-S_2 transition is expected to lie in the near- to mid-IR region (1000-8000 cm^{-1}) [84,118], but the high time resolution required (<50 fs) makes the envisaged VIS-pump/IR-probe spectroscopy challenging.

Like mutation effects discussed in chapter III, pH is known to induce small shifts in the ASR absorption maximum wavelength [124]. A new computational protocol has been devised and successfully applied to determine the molecular origin of such a pH effect [125]. The next step, still ongoing, focuses on the pH effect on the ESL. Preliminary results point to a bi-exponential decay from S_1, modulated by its pH-dependent interaction with S_2. Further upcoming developments relate to computing the excited state vibrational spectra of the rPSB, in relation with the very informative femtosecond data [91,111], and a possible inclusion of the dynamic polarisation of the nearest neighbour residues [15,74,75]. Unlike the here reported transient spectroscopies, ultrafast X-ray diffraction has the potential of revealing the detailed dynamic structural and electronic changes of the rPSB and its nearest environment, provided these experiments be carried out under single photon excitation conditions [63,72,73,126].

Beyond the excited state lifetimes and vibrational coherences, another central property is the reaction quantum yield (IQY), for which we still have to understand and learn the lessons that the outstanding high values found in Rho and bR can teach us, when these are compared with the modest values obtained for the biomimetic switches in solution [20] or the low values (<2%) observed for the crowed alkenes designed as molecular rotary machine [26]. While it is generally accepted that the branching into forward and backward reaction takes place in the vicinity of the conical intersection [23], it remains to be rationalised how chemical substitutions and effects of the environment control the IQY. Femto- and attosecond photo-electron spectroscopy holds the promise to map out the wavepacket evolution across the CI in real time, and one of the main challenges for the next years will be to apply these emerging sophisticated tools for isolated chromophores in gas phase [127,128] and solution [129].

VI. Acknowledgements

The authors acknowledge financial support from the French-German ANR-DFG project "Femto-ASR", (ANR- 14-CE35-0015-01) and ANR support via grant No. ANR-11-JS04-010-01 "IPQCS", and the "Investissement d'Avenir" program: Labex NIE ANR- 11-LABX-0058_NIE, Labex CSC ANR-10-LABX-0026_CSC, Equipex UNION ANR-10- EQPX-52-01. Other funding came from the Université de Strasbourg for a USIAS Fellowship, from the "Alsace" region, the NSF Grant No. CHE-1710191, and the Italian MIUR for grant PRIN 2015. M.O acknowledges the Ohio Supercomputer Center, the Mésocentre of the Université de Strasbourg and CINECA for granted computer time. The Centre de Calcul Intensif d'Aix-Marseille is acknowledged for granting access to its high performance computing resources.

High quality samples for wild-type ASR and its mutants came from H. Kandori and K. Jung and their teams. The contributions of J. Brazard, A. Cheminal and O. Crégut are kindly acknowledged, as well as from S. Fusi, M. Paolino, L. Barneschi, E. Pieri, V. Ledentu and L. Pedraza González.

REFERENCES

[1] O.P. Ernst, D.T. Lodowski, M. Elstner, P. Hegemann, L.S. Brown, H. Kandori, Microbial and Animal Rhodopsins: Structures, Functions, and Molecular Mechanisms, Chem. Rev. 114 (2014) 126–163. https://doi.org/10.1021/cr4003769.

[2] M. Kumauchi, T.G. Ebrey, Visual Pigments as Photoreceptors, in: Handb. Photosensory Recept., John Wiley & Sons, Ltd, 2005: pp. 43–76. https://doi.org/10.1002/352760510X.ch3.

[3] E.G. Govorunova, O.A. Sineshchekov, H. Li, J.L. Spudich, Microbial Rhodopsins: Diversity, Mechanisms, and Optogenetic Applications, Annu. Rev. Biochem. 86 (2017) 845–872. https://doi.org/10.1146/annurev-biochem-101910-144233.

[4] V. Bonačić-Koutecký, J. Köhler, J. Michl, Prediction of structural and environmental effects on the S1-S0 energy gap and jump probability in double-bond cis—trans photoisomerization, Chem. Phys. Lett. 104 (1984) 440–443. https://doi.org/10.1016/0009-2614(84)85619-5.

[5] A. Cembran, F. Bernardi, M. Olivucci, M. Garavelli, The retinal chromophore/chloride ion pair: Structure of the photo isomerization path and interplay of charge transfer and covalent states, Proc. Natl. Acad. Sci. U. S. A. 102 (2005) 6255–6260.

[6] A. Wand, I. Gdor, J.Y. Zhu, M. Sheves, S. Ruhman, Shedding New Light on Retinal Protein Photochemistry, Annu. Rev. Phys. Chem. Vol 64. 64 (2013) 437–458.

[7] R. Diller, Primary Reactions in Retinal Proteins, in: M. Braun, P. Gilch, W. Zinth (Eds.), Biol. Med. Phys. Biomed. Eng., Springer, Berlin Heidelberg, 2008: pp. 243–273.

[8] H. Kandori, Y. Katsuta, M. Ito, H. Sasabe, Femtosecond fluorescence study of the rhodopsin chromophore in solution, J. Am. Chem. Soc. 117 (1995) 2669–2670. https://doi.org/10.1021/ja00114a040.

[9] P. Hamm, M. Zurek, T. Röschinger, H. Patzelt, D. Oesterhelt, W. Zinth, Femtosecond spectroscopy of the photoisomerisation of the protonated Schiff base of all-trans retinal, Chem. Phys. Lett. 263 (1996) 613–621. https://doi.org/10.1016/S0009-2614(96)01269-9.

[10] G. Zgrablic, K. Voitchovsky, M. Kindermann, S. Haacke, M. Chergui, Ultrafast excited state dynamics of the protonated Schiff base of all-trans retinal in solvents, Biophys. J. 88 (2005) 2779–2788. https://doi.org/10.1529/biophysj.104.046094.

[11] T. Sovdat, G. Bassolino, M. Liebel, C. Schnedermann, S.P. Fletcher, P. Kukura, Backbone Modification of Retinal Induces Protein-like Excited State Dynamics in Solution, J. Am. Chem. Soc. 134 (2012) 8318–8320. https://doi.org/10.1021/ja3007929.

[12] S.L. Logunov, L. Song, M.A. El-Sayed, Excited-State Dynamics of a Protonated Retinal Schiff Base in Solution, J. Phys. Chem. 100 (1996) 18586–18591. https://doi.org/10.1021/jp962046d.

[13] J.P. Kraack, T. Buckup, M. Motzkus, Vibrational analysis of excited and ground electronic states of all-trans retinal protonated Schiff-base, Phys. Chem. Chem. Phys. 13 (2011) 21402–21410.

[14] J.P. Kraack, T. Buckup, M. Motzkus, Coherent High-Frequency Vibrational Dynamics in the Excited Electronic State of All-Trans Retinal Derivatives, J. Phys. Chem. Lett. 4 (2013) 383–387. https://doi.org/10.1021/jz302001m.

[15] H.V. Kiefer, E. Gruber, J. Langeland, P.A. Kusochek, A.V. Bochenkova, L.H. Andersen, Intrinsic photoisomerization dynamics of protonated Schiff-base retinal, Nat. Commun. 10 (2019) 1210. https://doi.org/10.1038/s41467-019-09225-7.

[16] M. Klessinger, Conical Intersections and the Mechanism of Singlet Photoreactions, Angew. Chem. Int. Ed. Engl. 34 (1995) 549–551. https://doi.org/10.1002/anie.199505491.

[17] B.G. Levine, T.J. Martínez, Isomerization Through Conical Intersections, Annu. Rev. Phys. Chem. 58 (2007) 613–634. https://doi.org/10.1146/annurev.physchem.57.032905.104612.

[18] T. Sovdat, G. Bassolino, M. Liebel, C. Schnedermann, S.P. Fletcher, P. Kukura, Backbone Modification of Retinal Induces Protein-like Excited State Dynamics in Solution, J. Am. Chem. Soc. 134 (2012) 8318–8320. https://doi.org/10.1021/ja3007929.

[19] A. Cheminal, J. Léonard, S.-Y. Kim, K.-H. Jung, H. Kandori, S. Haacke, 100 fs photo-isomerization with vibrational coherences but low quantum yield in Anabaena Sensory Rhodopsin, Phys. Chem. Chem. Phys. 17 (2015) 25429–25439. https://doi.org/10.1039/c5cp04353k.

[20] M. Gueye, M. Paolino, E. Gindensperger, S. Haacke, M. Olivucci, J. Léonard, Vibrational coherence and quantum yield of retinal-chromophore-inspired molecular switches, Faraday Discuss. 221 (2020) 299–321. https://doi.org/10.1039/C9FD00062C.
[21] G. Zgrablić, A.M. Novello, F. Parmigiani, Population Branching in the Conical Intersection of the Retinal Chromophore Revealed by Multipulse Ultrafast Optical Spectroscopy, J. Am. Chem. Soc. 134 (2012) 955–961. https://doi.org/10.1021/ja205763x.
[22] A. Valentini, D. Rivero, F. Zapata, C. García-Iriepa, M. Marazzi, R. Palmeiro, I. Fdez. Galván, D. Sampedro, M. Olivucci, L.M. Frutos, Optomechanical Control of Quantum Yield in Trans–Cis Ultrafast Photoisomerization of a Retinal Chromophore Model, Angew. Chem. Int. Ed. 56 (2017) 3842–3846. https://doi.org/10.1002/anie.201611265.
[23] C. Schnedermann, X. Yang, M. Liebel, K.M. Spillane, J. Lugtenburg, I. Fernández, A. Valentini, I. Schapiro, M. Olivucci, P. Kukura, R.A. Mathies, Evidence for a vibrational phase-dependent isotope effect on the photochemistry of vision, Nat. Chem. (2018). https://doi.org/10.1038/s41557-018-0014-y.
[24] H. Kandori, Retinal Proteins: Photochemistry and Optogenetics, Bull. Chem. Soc. Jpn. 93 (2020) 76–85. https://doi.org/10.1246/bcsj.20190292.
[25] D. Maclaurin, V. Venkatachalam, H. Lee, A.E. Cohen, Mechanism of voltage-sensitive fluorescence in a microbial rhodopsin, Proc. Natl. Acad. Sci. 110 (2013) 5939–5944. https://doi.org/10.1073/pnas.1215595110.
[26] D. Roke, S.J. Wezenberg, B.L. Feringa, Molecular rotary motors: Unidirectional motion around double bonds, Proc. Natl. Acad. Sci. 115 (2018) 9423–9431. https://doi.org/10.1073/pnas.1712784115.
[27] T. Okada, M. Sugihara, A.-N. Bondar, M. Elstner, P. Entel, V. Buss, The Retinal Conformation and its Environment in Rhodopsin in Light of a New 2.2Å Crystal Structure, J. Mol. Biol. 342 (2004) 571–583. https://doi.org/10.1016/j.jmb.2004.07.044.
[28] H. Luecke, B. Schobert, H.-T. Richter, J.-P. Cartailler, J.K. Lanyi, Structure of bacteriorhodopsin at 1.55 Å resolution 1, J. Mol. Biol. 291 (1999) 899–911. https://doi.org/10.1006/jmbi.1999.3027.
[29] R. Mathies, A.R. Oseroff, L. Stryer, Rapid-flow resonance Raman spectroscopy of photolabile molecules: rhodopsin and isorhodopsin, Proc. Natl. Acad. Sci. 73 (1976) 1–5.
[30] G. Eyring, B. Curry, A. Broek, J. Lugtenburg, R. Mathies, Assignment and interpretation of hydrogen out-of-plane vibrations in the resonance Raman spectra of rhodopsin and bathorhodopsin, Biochemistry. 21 (1982) 384–393. https://doi.org/10.1021/bi00531a028.
[31] R.W. Schoenlein, L.A. Peteanu, R.A. Mathies, C.V. Shank, The first step in vision: Femtosecond Isomerization of rhodopsin, Science. 254 (1991) 412–415.
[32] J.E. Kim, R.A. Mathies, Anti-stokes Raman study of vibrational cooling dynamics in the primary photochemistry of rhodopsin, J Phys Chem A. 106 (2002) 8508–15. https://doi.org/10.1021/jp021069r.
[33] Y. Hontani, M. Broser, M. Luck, J. Weißenborn, M. Kloz, P. Hegemann, J.T.M. Kennis, Dual Photoisomerization on Distinct Potential Energy Surfaces in a UV-Absorbing Rhodopsin, J. Am. Chem. Soc. 142 (2020) 11464–11473. https://doi.org/10.1021/jacs.0c03229.
[34] G.I. Groma, A. Colonna, J.C. Lambry, J.W. Petrich, G. Váró, M. Joffre, M.H. Vos, J.-L. Martin, Resonant optical rectification in bacteriorhodopsin, Proc Nat Acad Sci. 101 (2004) 7971–7975.
[35] R. Mathies, L. Stryer, Retinal has a highly dipolar vertically excited singlet state: implications for vision, Proc. Natl. Acad. Sci. 73 (1976) 2169–2173. https://doi.org/10.1073/pnas.73.7.2169.
[36] H. Houjou, Y. Inoue, M. Sakurai, Physical Origin of the Opsin Shift of Bacteriorhodopsin. Comprehensive Analysis Based on Medium Effect Theory of Absorption Spectra, J. Am. Chem. Soc. 120 (1998) 4459–4470. https://doi.org/10.1021/ja973941t.
[37] R. Rajamani, J. Gao, Combined QM/MM study of the opsin shift in bacteriorhodopsin, J. Comput. Chem. 23 (2002) 96–105. https://doi.org/10.1002/jcc.1159.
[38] C. Punwong, J. Owens, T.J. Martínez, Direct QM/MM Excited-State Dynamics of Retinal Protonated Schiff Base in Isolation and Methanol Solution, J. Phys. Chem. B. 119 (2015) 704–714. https://doi.org/10.1021/jp5038798.

[39] M. Mališ, J. Novak, G. Zgrablić, F. Parmigiani, N. Došlić, Mechanism of ultrafast non-reactive deactivation of the retinal chromophore in non-polar solvents, Phys. Chem. Chem. Phys. 19 (2017) 25970–25978. https://doi.org/10.1039/C7CP03293E.
[40] K.A. Freedman, R.S. Becker, Comparative investigation of the photoisomerization of the protonated and unprotonated n-butylamine Schiff bases of 9-cis-, 11-cis-, 13-cis-, and all-trans-retinals, J. Am. Chem. Soc. 108 (1986) 1245–1251. https://doi.org/10.1021/ja00266a020.
[41] R.S. Becker, K. Freedman, A comprehensive investigation of the mechanism and photophysics of isomerization of a protonated and unprotonated Schiff base of 11-cis-retinal, J. Am. Chem. Soc. 107 (1985) 1477–1485. https://doi.org/10.1021/ja00292a005.
[42] Y. Koyama, K. Kubo, M. Komori, H. Yasuda, Y. Mukai, EFFECT OF PROTONATION ON THE ISOMERIZATION PROPERTIES OF n-BUTYLAMINE SCHIFF BASE OF ISOMERIC RETINAL AS REVEALED BY DIRECT HPLC ANALYSES: SELECTION OF ISOMERIZATION PATHWAYS BY RETINAL PROTEINS, Photochem. Photobiol. 54 (1991) 433–443. https://doi.org/10.1111/j.1751-1097.1991.tb02038.x.
[43] P. Hamm, M. Zurek, T. Röschinger, H. Patzelt, D. Oesterhelt, W. Zinth, Femtosecond spectroscopy of the photoisomerization of the protonated Schiff base of all-trans retinal, Chem Phys Lett. 263 (1996) 613–621.
[44] G. Zgrablic, S. Haacke, M. Chergui, Heterogeneity and Relaxation Dynamics of the Photoexcited Retinal Schiff Base Cation in Solution, J. Phys. Chem. B. 113 (2009) 4384–4393. https://doi.org/10.1021/jp8077216.
[45] G. Bassolino, T. Sovdat, A. Soares Duarte, J.M. Lim, C. Schnedermann, M. Liebel, B. Odell, T.D.W. Claridge, S.P. Fletcher, P. Kukura, Barrierless Photoisomerization of 11-cis Retinal Protonated Schiff Base in Solution, J. Am. Chem. Soc. 137 (2015) 12434–12437. https://doi.org/10.1021/jacs.5b06492.
[46] L. Andersen, I. Nielsen, M. Kristensen, M. El Ghazaly, S. Haacke, M. Nielsen, M. Petersen, Absorption of Schiff-base retinal chromophores in vacuo, J. Am. Chem. Soc. 127 (2005) 12347–12350. https://doi.org/10.1021/ja051638j.
[47] J. Langeland Knudsen, A. Kluge, A. V. Bochenkova, H. V. Kiefer, L. H. Andersen, The UV-visible action-absorption spectrum of all- trans and 11- cis protonated Schiff base retinal in the gas phase, Phys. Chem. Chem. Phys. 20 (2018) 7190–7194. https://doi.org/10.1039/C7CP07512J.
[48] D. Oesterhelt, W. Stoeckenius, Rhodopsin-like Protein from the Purple Membrane of Halobacterium halobium, Nature. New Biol. 233 (1971) 149–152. https://doi.org/10.1038/newbio233149a0.
[49] M.C. Nuss, W. Zinth, W. Kaiser, E. Kölling, D. Oesterhelt, Femtosecond spectroscopy of the first events of the photochemical cycle in bacteriorhodopsin, Chem Phys Lett. 117 (1985) 1–7.
[50] H.J. Polland, M.A. Franz, W. Zinth, W. Kaiser, E. Kölling, D. Oesterhelt, Early picosecond events in the photocycle of bacteriorhodopsin, Biophys J. 49 (1986) 651–662.
[51] M. Du, G.R. Fleming, Femtosecond time-resolved fluorescence spectroscopy of bacteriorhodopsin: Direct observation of excited state dynamics in the primary step of the proton pump cycle, Biophys. Chem. 48 (1993) 101–111. https://doi.org/10.1016/0301-4622(93)85002-Y.
[52] J. Herbst, K. Heyne, R. Diller, Femtosecond infrared spectroscopy of bacteriorhodopsin chromophore isomerization, Science. 297 (2002) 822–825.
[53] J. Tittor, D. Oesterhelt, The quantum yield of bacteriorhodopsin, FEBS Lett. 263 (1990) 269–273. https://doi.org/10.1016/0014-5793(90)81390-A.
[54] R. Govindjee, S.P. Balashov, T.G. Ebrey, Quantum efficiency of the photochemical cycle of bacteriorhodopsin, Biophys. J. 58 (1990) 597–608. https://doi.org/10.1016/S0006-3495(90)82403-6.
[55] G. Schneider, R. Diller, M. Stockburger, Photochemical quantum yield of bacteriorhodopsin from resonance Raman scattering as a probe for photolysis, Chem. Phys. 131 (1989) 17–29. https://doi.org/10.1016/0301-0104(89)87078-8.

[56] L. Song, M.A. El-Sayed, J.K. Lanyi, Protein Catalysis of the Retinal Subpicosecond Photoisomerization in the Primary Process of Bacteriorhodopsin Photosynthesis, Science. 261 (1993) 891–894. https://doi.org/10.1126/science.261.5123.891.
[57] S.L. Logunov, M.A. ElSayed, L. Song, J.K. Lanyi, Photoisomerization quantum yield and apparent energy content of the K intermediate in the photocycles of bacteriorhodopsin, its mutants D85N, R82Q, and D212N, and deionized blue bacteriorhodopsin, J. Phys. Chem. 100 (1996) 2391–2398.
[58] T. Kobayashi, M. Terauchi, T. Kouyama, M. Yoshizawa, M. Taiji, Femtosecond spectroscopy of acidified and neutral bacteriorhodopsin, 1403 (1991) 407–416. https://doi.org/10.1117/12.57310.
[59] J.T.M. Kennis, D.S. Larsen, K. Ohta, M.T. Facciotti, R.M. Glaeser, G.R. Fleming, Ultrafast Protein Dynamics of Bacteriorhodopsin Probed by Photon Echo and Transient Absorption Spectroscopy, J. Phys. Chem. B. 106 (2002) 6067–6080. https://doi.org/10.1021/jp014681b.
[60] K. Inoue, H. Ono, R. Abe-Yoshizumi, S. Yoshizawa, H. Ito, K. Kogure, H. Kandori, A light-driven sodium ion pump in marine bacteria, Nat. Commun. 4 (2013) 1678. https://doi.org/10.1038/ncomms2689.
[61] H.E. Kato, K. Inoue, R. Abe-Yoshizumi, Y. Kato, H. Ono, M. Konno, S. Hososhima, T. Ishizuka, M.R. Hoque, H. Kunitomo, J. Ito, S. Yoshizawa, K. Yamashita, M. Takemoto, T. Nishizawa, R. Taniguchi, K. Kogure, A.D. Maturana, Y. Iino, H. Yawo, R. Ishitani, H. Kandori, O. Nureki, Structural basis for Na+ transport mechanism by a light-driven Na+ pump, Nature. 521 (2015) 48–53. https://doi.org/10.1038/nature14322.
[62] I. Gushchin, V. Shevchenko, V. Polovinkin, V. Borshchevskiy, P. Buslaev, E. Bamberg, V. Gordeliy, Structure of the light-driven sodium pump KR2 and its implications for optogenetics, FEBS J. 283 (2016) 1232–1238. https://doi.org/10.1111/febs.13585.
[63] P. Skopintsev, D. Ehrenberg, T. Weinert, D. James, R.K. Kar, P.J.M. Johnson, D. Ozerov, A. Furrer, I. Martiel, F. Dworkowski, K. Nass, G. Knopp, C. Cirelli, C. Arrell, D. Gashi, S. Mous, M. Wranik, T. Gruhl, D. Kekilli, S. Brünle, X. Deupi, G.F.X. Schertler, R.M. Benoit, V. Panneels, P. Nogly, I. Schapiro, C. Milne, J. Heberle, J. Standfuss, Femtosecond-to-millisecond structural changes in a light-driven sodium pump, Nature. (2020) 1–5. https://doi.org/10.1038/s41586-020-2307-8.
[64] Y. Hontani, K. Inoue, M. Kloz, Y. Kato, H. Kandori, J.T.M. Kennis, The photochemistry of sodium ion pump rhodopsin observed by watermarked femto- to submillisecond stimulated Raman spectroscopy, Phys. Chem. Chem. Phys. 18 (2016) 24729–24736. https://doi.org/10.1039/C6CP05240A.
[65] S. Tahara, S. Takeuchi, R. Abe-Yoshizumi, K. Inoue, H. Ohtani, H. Kandori, T. Tahara, Ultrafast Photoreaction Dynamics of a Light-Driven Sodium-Ion-Pumping Retinal Protein from *Krokinobacter eikastus* Revealed by Femtosecond Time-Resolved Absorption Spectroscopy, J. Phys. Chem. Lett. 6 (2015) 4481–4486. https://doi.org/10.1021/acs.jpclett.5b01994.
[66] S. Tahara, S. Takeuchi, R. Abe-Yoshizumi, K. Inoue, H. Ohtani, H. Kandori, T. Tahara, Origin of the Reactive and Nonreactive Excited States in the Primary Reaction of Rhodopsins: pH Dependence of Femtosecond Absorption of Light-Driven Sodium Ion Pump Rhodopsin KR2, J. Phys. Chem. B. 122 (2018) 4784–4792. https://doi.org/10.1021/acs.jpcb.8b01934.
[67] M.O. Lenz, R. Huber, B. Schmidt, P. Gilch, R. Kalmbach, M. Engelhard, J. Wachtveitl, First Steps of Retinal Photoisomerization in Proteorhodopsin, Biophys. J. 91 (2006) 255–262. https://doi.org/10.1529/biophysj.105.074690.
[68] T. Nakamura, S. Takeuchi, M. Shibata, M. Demura, H. Kandori, T. Tahara, Ultrafast Pump−Probe Study of the Primary Photoreaction Process in pharaonis Halorhodopsin: Halide Ion Dependence and Isomerization Dynamics, J. Phys. Chem. B. 112 (2008) 12795–12800. https://doi.org/10.1021/jp803282s.
[69] C.-F. Chang, H. Kuramochi, M. Singh, R. Abe-Yoshizumi, T. Tsukuda, H. Kandori, T. Tahara, Acid–base equilibrium of the chromophore counterion results in distinct photoisomerization reactivity in the primary event of proteorhodopsin, Phys. Chem. Chem. Phys. 21 (2019) 25728–25734. https://doi.org/10.1039/C9CP04991F.

[70] M. Karasuyama, K. Inoue, R. Nakamura, H. Kandori, I. Takeuchi, Understanding Colour Tuning Rules and Predicting Absorption Wavelengths of Microbial Rhodopsins by Data-Driven Machine-Learning Approach, Sci. Rep. 8 (2018) 15580. https://doi.org/10.1038/s41598-018-33984-w.
[71] B.R. Rost, F. Schneider-Warme, D. Schmitz, P. Hegemann, Optogenetic Tools for Subcellular Applications in Neuroscience, Neuron. 96 (2017) 572–603. https://doi.org/10.1016/j.neuron.2017.09.047.
[72] P. Nogly, T. Weinert, D. James, S. Carbajo, D. Ozerov, A. Furrer, D. Gashi, V. Borin, P. Skopintsev, K. Jaeger, K. Nass, P. Båth, R. Bosman, J. Koglin, M. Seaberg, T. Lane, D. Kekilli, S. Brünle, T. Tanaka, W. Wu, C. Milne, T. White, A. Barty, U. Weierstall, V. Panneels, E. Nango, S. Iwata, M. Hunter, I. Schapiro, G. Schertler, R. Neutze, J. Standfuss, Retinal isomerization in bacteriorhodopsin captured by a femtosecond x-ray laser, Science. (2018) eaat0094. https://doi.org/10.1126/science.aat0094.
[73] G. Nass Kovacs, J.-P. Colletier, M.L. Grünbein, Y. Yang, T. Stensitzki, A. Batyuk, S. Carbajo, R.B. Doak, D. Ehrenberg, L. Foucar, R. Gasper, A. Gorel, M. Hilpert, M. Kloos, J.E. Koglin, J. Reinstein, C.M. Roome, R. Schlesinger, M. Seaberg, R.L. Shoeman, M. Stricker, S. Boutet, S. Haacke, J. Heberle, K. Heyne, T. Domratcheva, T.R.M. Barends, I. Schlichting, Three-dimensional view of ultrafast dynamics in photoexcited bacteriorhodopsin, Nat. Commun. 10 (2019) 3177. https://doi.org/10.1038/s41467-019-10758-0.
[74] S. Schenkl, F. van Mourik, G. van der Zwan, S. Haacke, M. Chergui, Probing the ultrafast charge translocation of photoexcited retinal in bacteriorhodopsin, Science. 309 (2005) 917–920. https://doi.org/10.1126/science.1111482.
[75] J. Léonard, E. Portuondo-Campa, A. Cannizzo, F. van Mourik, G. van der Zwan, J. Tittor, S. Haacke, M. Chergui, Functional electric field changes in photoactivated proteins revealed by ultrafast Stark spectroscopy of the Trp residues, Proc. Natl. Acad. Sci. U. S. A. 106 (2009) 7718–7723. https://doi.org/10.1073/pnas.0812877106.
[76] S. Tahara, H. Kuramochi, S. Takeuchi, T. Tahara, Protein Dynamics Preceding Photoisomerization of the Retinal Chromophore in Bacteriorhodopsin Revealed by Deep-UV Femtosecond Stimulated Raman Spectroscopy, J. Phys. Chem. Lett. 10 (2019) 5422–5427. https://doi.org/10.1021/acs.jpclett.9b02283.
[77] P. Tavan, K. Schulten, Electronic excitations in finite and infinite polyenes, Phys. Rev. B. 36 (1987) 4337–4358. https://doi.org/10.1103/PhysRevB.36.4337.
[78] K.C. Hasson, F. Gai, P.A. Anfinrud, The photoisomerization of retinal in bacteriorhodopsin: Experimental evidence for a three-state model, Proc. Natl. Acad. Sci. 93 (1996) 15124–15129.
[79] A. Muñoz-Losa, M.E. Martín, I.Fdez. Galván, M.L. Sánchez, M.A. Aguilar, Solvent Effects on the Radiative and Nonradiative Decay of a Model of the Rhodopsin Chromophore, J. Chem. Theory Comput. 7 (2011) 4050–4059.
[80] R. González-Luque, M. Garavelli, F. Bernardi, M. Merchán, M.A. Robb, M. Olivucci, Computational evidence in favor of a two-state, two-mode model of the retinal chromophore photoisomerization, Proc. Natl. Acad. Sci. 97 (2000) 9379–9384. https://doi.org/10.1073/pnas.97.17.9379.
[81] A. Cembran, R. González-Luque, L. Serrano-Andrés, M. Merchán, M. Garavelli, About the intrinsic photochemical properties of the 11-cis retinal chromophore: computational clues for a trap state and a lever effect in Rhodopsin catalysis, Theor. Chem. Acc. 118 (2007) 173–183. https://doi.org/10.1007/s00214-007-0259-9.
[82] J.P. Kraack, T. Buckup, M. Motzkus, Evidence for the Two-State-Two-Mode model in retinal protonated Schiff-bases from pump degenerate four-wave-mixing experiments, Phys. Chem. Chem. Phys. 14 (2012) 13979–13988. https://doi.org/10.1039/c2cp42248d.
[83] S. Gozem, H.L. Luk, I. Schapiro, M. Olivucci, Theory and Simulation of the Ultrafast Double-Bond Isomerization of Biological Chromophores, Chem. Rev. 117 (2017) 13502–13565. https://doi.org/10.1021/acs.chemrev.7b00177.

[84] M. Manathunga, X. Yang, Y. Orozco-Gonzalez, M. Olivucci, Impact of Electronic State Mixing on the Photoisomerization Time Scale of the Retinal Chromophore, J. Phys. Chem. Lett. 8 (2017) 5222–5227. https://doi.org/10.1021/acs.jpclett.7b02344.
[85] M. Manathunga, X. Yang, M. Olivucci, Electronic State Mixing Controls the Photoreactivity of a Rhodopsin with all-trans Chromophore Analogues, J. Phys. Chem. Lett. 9 (2018) 6350–6355. https://doi.org/10.1021/acs.jpclett.8b02550.
[86] H.L. Luk, F. Melaccio, S. Rinaldi, S. Gozem, M. Olivucci, Molecular bases for the selection of the chromophore of animal rhodopsins, Proc Natl Acad Sci U A. 112 (2015) 15297–302. https://doi.org/10.1073/pnas.1510262112.
[87] S. Gozem, P.J.M. Johnson, A. Halpin, H.L. Luk, T. Morizumi, V.I. Prokhorenko, O.P. Ernst, M. Olivucci, R.J.D. Miller, Excited-State Vibronic Dynamics of Bacteriorhodopsin from Two-Dimensional Electronic Photon Echo Spectroscopy and Multiconfigurational Quantum Chemistry, J. Phys. Chem. Lett. (2020) 3889–3896. https://doi.org/10.1021/acs.jpclett.0c01063.
[88] B. Demoulin, S.F. Altavilla, I. Rivalta, M. Garavelli, Fine Tuning of Retinal Photoinduced Decay in Solution, J. Phys. Chem. Lett. 8 (2017) 4407–4412. https://doi.org/10.1021/acs.jpclett.7b01780.
[89] S. Smith, J.A. Pardoen, J. Lugtenburg, R.A. Mathies, Vibrational analysis of the 13-cis-Retinal Chromophore in dark-Adapted Bacteriorhodopsin, J. Phys. Chemstry. 91 (1987) 804–819.
[90] A. Wand, B. Loevsky, N. Friedman, M. Sheves, S. Ruhman, Probing Ultrafast Photochemistry of Retinal Proteins in the Near-IR: Bacteriorhodopsin and Anabaena Sensory Rhodopsin vs Retinal Protonated Schiff Base in Solution, J. Phys. Chem. B. 117 (2013) 4670–4679.
[91] P. Pratim Roy, Y. Kato, R. Abe-Yoshizumi, E. Pieri, N. Ferré, H. Kandori, T. Buckup, Mapping the ultrafast vibrational dynamics of all- trans and 13- cis retinal isomerization in Anabaena Sensory Rhodopsin, Phys. Chem. Chem. Phys. 20 (2018) 30159–30173. https://doi.org/10.1039/C8CP05469J.
[92] O. Weingart, I. Schapiro, V. Buss, Photochemistry of Visual Pigment Chromophore Models by Ab Initio Molecular Dynamics, J. Phys. Chem. B. 111 (2007) 3782–3788. https://doi.org/10.1021/jp0683216.
[93] Q. Wang, R.W. Schoenlein, L.A. Peteanu, R.A. Mathies, C.V. Shank, Vibrationally coherent photochemistry in the femtosecond primary event of vision, Science. 266 (1994) 422–4.
[94] D. Polli, P. Altoe, O. Weingart, K.M. Spillane, C. Manzoni, D. Brida, G. Tomasello, G. Orlandi, P. Kukura, R.A. Mathies, M. Garavelli, G. Cerullo, Conical intersection dynamics of the primary photoisomerization event in vision, Nature. 467 (2010) 440-U88.
[95] P.J. Johnson, A. Halpin, T. Morizumi, V.I. Prokhorenko, O.P. Ernst, R.J. Miller, Local vibrational coherences drive the primary photochemistry of vision, Nat Chem. 7 (2015) 980–6. https://doi.org/10.1038/nchem.2398.
[96] P.J.M. Johnson, M.H. Farag, A. Halpin, T. Morizumi, V.I. Prokhorenko, J. Knoester, T.L.C. Jansen, O.P. Ernst, R.J.D. Miller, The Primary Photochemistry of Vision Occurs at the Molecular Speed Limit, J. Phys. Chem. B. 121 (2017) 4040–4047. https://doi.org/10.1021/acs.jpcb.7b02329.
[97] A. Wand, R. Rozin, T. Eliash, K.-H. Jung, M. Sheves, S. Ruhman, Asymmetric Toggling of a Natural Photoswitch: Ultrafast Spectroscopy of Anabaena Sensory Rhodopsin, J. Am. Chem. Soc. 133 (2011) 20922–20932. https://doi.org/10.1021/ja208371g.
[98] G. Bassolino, T. Sovdat, M. Liebel, C. Schnedermann, B. Odell, T.D.W. Claridge, P. Kukura, S.P. Fletcher, Synthetic Control of Retinal Photochemistry and Photophysics in Solution, J. Am. Chem. Soc. 136 (2014) 2650–2658. https://doi.org/10.1021/ja4121814.
[99] K.-H. Jung, V.D. Trivedi, J.L. Spudich, Demonstration of a sensory rhodopsin in eubacteria, Mol. Microbiol. 47 (2003) 1513–1522. https://doi.org/10.1046/j.1365-2958.2003.03395.x.
[100] A. Kawanabe, H. Kandori, Photoreactions and structural changes of anabaena sensory rhodopsin, Sens. Basel. 9 (2009) 9741–804. https://doi.org/10.3390/s91209741.
[101] L. Vogeley, O.A. Sineshchekov, V.D. Trivedi, J. Sasaki, J.L. Spudich, H. Luecke, Anabaena Sensory Rhodopsin: A Photochromic Color Sensor at 2.0 Å, Science. 306 (2004) 1390–1393. https://doi.org/10.1126/science.1103943.

[102] A. Kawanabe, Y. Furutani, K.-H. Jung, H. Kandori, FTIR Study of the Photoisomerization Processes in the 13- *cis* and All- *trans* Forms of *Anabaena* Sensory Rhodopsin at 77 K †, Biochemistry. 45 (2006) 4362–4370. https://doi.org/10.1021/bi052324b.
[103] I. Schapiro, S. Ruhman, Ultrafast photochemistry of Anabaena Sensory Rhodopsin: Experiment and theory, Biochim. Biophys. Acta BBA - Bioenerg. 1837 (2014) 589–597. https://doi.org/10.1016/j.bbabio.2013.09.014.
[104] A. Strambi, B. Durbeej, N. Ferré, M. Olivucci, Anabaena sensory rhodopsin is a light-driven unidirectional rotor, Proc. Natl. Acad. Sci. 107 (2010) 21322–21326. https://doi.org/10.1073/pnas.1015085107.
[105] D. Agathangelou, Y. Orozco-Gonzalez, M. del Carmen Marin, P.P. Roy, J. Brazard, H. Kandori, K.H. Jung, J. Léonard, T. Buckup, N. Ferre, M. Olivucci, S. Haacke, Effect of point mutations on the ultrafast photo-isomerization of Anabaena sensory rhodopsin, Faraday Discuss. 207 (2018) 55–75. https://doi.org/10.1039/c7fd00200a.
[106] Y. Orozco-Gonzalez, M. Manathunga, M. del C. Marin, D. Agathangelou, K.-H. Jung, F. Melaccio, N. Ferre, S. Haacke, K. Coutinho, S. Canuto, M. Olivucci, An Average Solvent Electrostatic Configuration Protocol for QM/MM Free Energy Optimization: Implementation and Application to Rhodopsin Systems, J. Chem. Theory Comput. 13 (2017) 6391–6404. https://doi.org/10.1021/acs.jctc.7b00860.
[107] J. Hauer, T. Buckup, M. Motzkus, Pump-degenerate four wave mixing as a technique for analyzing structural and electronic evolution: Multidimensional time-resolved dynamics near a conical intersection, J. Phys. Chem. A. 111 (2007) 10517–10529.
[108] T. Buckup, J. Hauer, J. Mohring, M. Motzkus, Multidimensional spectroscopy of beta-carotene: Vibrational cooling in the excited state, Arch. Biochem. Biophys. 483 (2009) 219–223.
[109] T. Buckup, J. Léonard, Multidimensional Vibrational Coherence Spectroscopy, Top. Curr. Chem. 376 (2018). https://doi.org/10.1007/s41061-018-0213-4.
[110] T. Buckup, M. Motzkus, Multidimensional time-resolved spectroscopy of vibrational coherence in biopolyenes, Annu. Rev. Phys. Chem. 65 (2015) 39–57.
[111] P.P. Roy, R. Abe-Yoshizumi, H. Kandori, T. Buckup, Point Mutation of *Anabaena* Sensory Rhodopsin Enhances Ground-State Hydrogen Out-of-Plane Wag Raman Activity, J. Phys. Chem. Lett. 10 (2019) 1012–1017. https://doi.org/10.1021/acs.jpclett.8b03805.
[112] M.D.C. Marin, D. Agathangelou, Y. Orozco-Gonzalez, A. Valentini, Y. Kato, R. Abe-Yoshizumi, H. Kandori, A. Choi, K.-H. Jung, S. Haacke, M. Olivucci, Fluorescence enhancement of a microbial rhodopsin via electronic reprogramming, J. Am. Chem. Soc. (2018). https://doi.org/10.1021/jacs.8b09311.
[113] F. Melaccio, M. Del Carmen Marin, A. Valentini, F. Montisci, S. Rinaldi, M. Cherubini, X. Yang, Y. Kato, M. Stenrup, Y. Orozco-Gonzalez, N. Ferre, H.L. Luk, H. Kandori, M. Olivucci, Toward Automatic Rhodopsin Modeling as a Tool for High-Throughput Computational Photobiology, J Chem Theory Comput. 12 (2016) 6020–6034. https://doi.org/10.1021/acs.jctc.6b00367.
[114] F. Lumento, V. Zanirato, S. Fusi, E. Busi, L. Latterini, F. Elisei, A. Sinicropi, T. Andruniów, N. Ferré, R. Basosi, M. Olivucci, Quantum Chemical Modeling and Preparation of a Biomimetic Photochemical Switch, Angew. Chem. 119 (2007) 418–424. https://doi.org/10.1002/ange.200602915.
[115] A. Sinicropi, E. Martin, M. Ryazantsev, J. Helbing, J. Briand, D. Sharma, J. Léonard, S. Haacke, A. Cannizzo, M. Chergui, V. Zanirato, S. Fusi, F. Santoro, R. Basosi, N. Ferre, M. Olivucci, An artificial molecular switch that mimics the visual pigment and completes its photocycle in picoseconds, Proc. Natl. Acad. Sci. U. S. A. 105 (2008) 17642–17647. https://doi.org/10.1073/pnas.0802376105.
[116] B.L. Feringa, The Art of Building Small: From Molecular Switches to Motors (Nobel Lecture), Angew. Chem. Int. Ed. 56 (2017) 11060–11078. https://doi.org/10.1002/anie.201702979.
[117] T.P. Sakmar, R.R. Franke, H.G. Khorana, Glutamic acid-113 serves as the retinylidene Schiff base counterion in bovine rhodopsin, Proc. Natl. Acad. Sci. 86 (1989) 8309–8313.

[118] M. Gueye, M. Manathunga, D. Agathangelou, Y. Orozco, M. Paolino, S. Fusi, S. Haacke, M. Olivucci, J. Léonard, Engineering the vibrational coherence of vision into a synthetic molecular device, Nat. Commun. 9 (2018) 313. https://doi.org/10.1038/s41467-017-02668-w.
[119] J. Briand, O. Braem, J. Rehault, J. Léonard, A. Cannizzo, M. Chergui, V. Zanirato, M. Olivucci, J. Helbing, S. Haacke, Coherent ultrafast torsional motion and isomerization of a biomimetic dipolar photoswitch, Phys. Chem. Chem. Phys. 12 (2010) 3178–3187. https://doi.org/10.1039/b918603d.
[120] A.D. Dunkelberger, R.D. Kieda, J.Y. Shin, R. Rossi Paccani, S. Fusi, M. Olivucci, F. Fleming Crim, Photoisomerization and Relaxation Dynamics of a Structurally Modified Biomimetic Photoswitch, J. Phys. Chem. A. 116 (2012) 3527–3533. https://doi.org/10.1021/jp300153a.
[121] J. Léonard, I. Schapiro, J. Briand, S. Fusi, R.R. Paccani, M. Olivucci, S. Haacke, Mechanistic Origin of the Vibrational Coherence Accompanying the Photoreaction of Biomimetic Molecular Switches, Chem.- Eur. J. 18 (2012) 15296–15304. https://doi.org/10.1002/chem.201201430.
[122] J. Léonard, J. Briand, S. Fusi, V. Zanirato, M. Olivucci, S. Haacke, Isomer-dependent vibrational coherence in ultrafast photoisomerization, New J. Phys. 15 (2013). https://doi.org/10.1088/1367-2630/15/10/105022.
[123] I. Schapiro, M. Gueye, M. Paolino, S. Fusi, G. Marchand, S. Haacke, M. Elena Martin, M. Huntress, V. P. Vysotskiy, V. Veryazov, J. Léonard, M. Olivucci, Synthesis, spectroscopy and QM/MM simulations of a biomimetic ultrafast light-driven molecular motor, Photochem. Photobiol. Sci. 18 (2019) 2259–2269. https://doi.org/10.1039/C9PP00223E.
[124] R. Rozin, A. Wand, K.H. Jung, S. Ruhman, M. Sheves, pH dependence of Anabaena sensory rhodopsin: retinal isomer composition, rate of dark adaptation, and photochemistry, J Phys Chem B. 118 (2014) 8995–9006. https://doi.org/10.1021/jp504688y.
[125] M. Stenrup, E. Pieri, V. Ledentu, N. Ferré, pH-Dependent absorption spectrum of a protein: a minimal electrostatic model of Anabaena sensory rhodopsin, Phys. Chem. Chem. Phys. 19 (2017) 14073–14084. https://doi.org/10.1039/C7CP00991G.
[126] M.L. Grünbein, M. Stricker, G. Nass Kovacs, M. Kloos, R.B. Doak, R.L. Shoeman, J. Reinstein, S. Lecler, S. Haacke, I. Schlichting, Illumination guidelines for ultrafast pump–probe experiments by serial femtosecond crystallography, Nat. Methods. (2020). https://doi.org/10.1038/s41592-020-0847-3.
[127] S. Adachi, T. Schatteburg, A. Humeniuk, R. Mitrić, T. Suzuki, Probing ultrafast dynamics during and after passing through conical intersections, Phys. Chem. Chem. Phys. (2019). https://doi.org/10.1039/C8CP04426K.
[128] A.D. Smith, E.M. Warne, D. Bellshaw, D.A. Horke, M. Tudorovskya, E. Springate, A.J.H. Jones, C. Cacho, R.T. Chapman, A. Kirrander, R.S. Minns, Mapping the Complete Reaction Path of a Complex Photochemical Reaction, Phys. Rev. Lett. 120 (2018) 183003. https://doi.org/10.1103/PhysRevLett.120.183003.
[129] J. Hummert, G. Reitsma, N. Mayer, E. Ikonnikov, M. Eckstein, O. Kornilov, Femtosecond Extreme Ultraviolet Photoelectron Spectroscopy of Organic Molecules in Aqueous Solution, J. Phys. Chem. Lett. 9 (2018) 6649–6655. https://doi.org/10.1021/acs.jpclett.8b02937.